# EXAFS Spectroelectrochemistry

LEE R. SHARPE

*Department of Chemistry, Grinnell College, Grinnell, Iowa 50112*

WILLIAM R. HEINEMAN* and R. C. ELDER*

*Department of Chemistry, University of Cincinnati, Cincinnati, Ohio 45221-0172*

*Received October 24, 1989 (Revised Manuscript Received January 30, 1990)*

## Contents



## I. Introduction

Spectroelectrochemistry combines a spectroscopic technique with an electrochemical technique, which allows one to obtain greater insight into a particular chemical system than either or both of the component techniques used separately. In a typical experiment, the electrochemical technique is used to control the oxidation state of the material of interest while it is probed spectroscopically. Several types of spectroscopy have been used in spectroelectrochemistry including ultraviolet, visible, infrared, Mössbauer, and Raman.[1-4] Unfortunately, these techniques do not provide direct structural information. X-ray absorption spectroscopy, XAS, allows one to determine the oxidation state of an absorbing atom in addition to the numbers and types of atom neighbors to the absorber and the corresponding interatomic distances (to about 4.0 Å). In combination with an electrochemical technique, the changes in bond length and coordination number with change in oxidation state can be directly ascertained in situ.

The standard XAS experiment involves the measurement of the absorption and/or fluorescence of a particular element in a molecule or condensed material as the energy of the incident X-rays is scanned through the absorption edge. The two regions of the X-ray spectrum of particular interest in XAS are shown in Figure 1. The first region, which is near the absorption edge, displays the structure resulting from X-ray absorption at energies sufficient to promote core electrons to unoccupied atomic or molecular orbitals. The most commonly used acronym for this structure is XANES, which is X-ray absorption near-edge structure. Another acronym is NEXAFS or near-edge X-ray absorption fine structure. The position of the edge rise and XANES can provide information concerning the oxidation state of the absorber and the identity of the neighbor atoms. The second region of interest extends approximately 1000 eV beyond the edge and is characterized by a series of oscillations in the X-ray absorption coefficient that arise from the interference of the outgoing photoelectron wave (created by the photoionization of the "absorbing atom") with itself after being back-scattered by neighboring atoms around the absorbing atom. These "wiggles" are referred to as EXAFS or extended X-ray absorption fine structure. Information concerning the number and identity of the neighboring atoms can be extracted from the magnitude of the oscillations and the energy dependence of the amplitude, respectively. The frequencies of the oscillations can be used to determine the distance between the absorber and its neighboring atoms. The details of XAS data reduction are beyond the scope of this paper, and the reader is referred to other papers discussing this topic.[5]

X-ray absorption spectroelectrochemistry provides a means to study the changes in the coordination environment around an absorbing center as a function of oxidation state. Given the considerable interest in the affect of geometric and electronic structure on electron-exchange reactions,[6] the utility of this technique becomes quite apparent. Through use of thin-layer electrochemical cells, which are relatively transparent to the "hard" X-rays utilized in the XAS experiment, EXAFS spctroelectrochemistry can be performed in situ. This has a significant advantage over other surface structure-sensitive techniques that require ultrahigh-vacuum conditions such as low-energy electron diffraction and Auger electron spectroscopy. There is the question in ex situ measurements whether the structure and oxidation state of the material of interest has changed upon removing it from the electrolyte and potential control.

In this review, we focus on the applications of in situ X-ray absorption spectroelectrochemistry to solutions,

0009-2665/90/0790-0705$09.50/0 

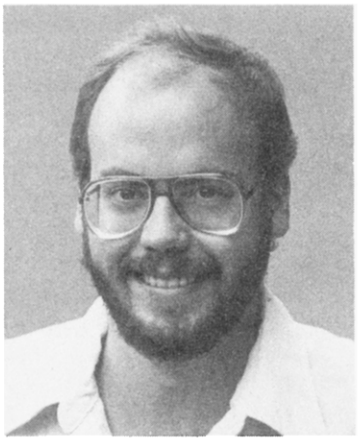

Lee R. Sharpe, a native of Wisconsin, received his A.B. in Chemistry from Ripon College, Ripon, WI, and his Ph.D. in Inorganic Chemistry from the University of Wisconsin—Madison with Arthur B. Ellis. He then went to the University of Cincinnati as a postdoctoral fellow to work with Professors R. C. Elder and W. R. Heineman on EXAFS spectroelectrochemistry. Presently, he is an Assistant Professor of Analytical Chemistry at Grinnell College, Grinnell, IA.

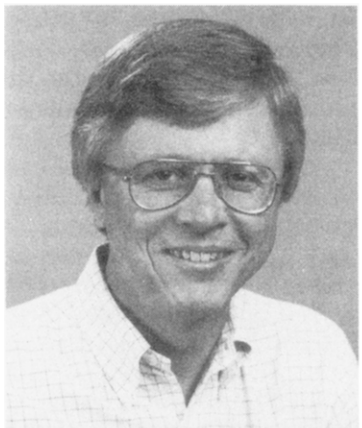

William R. Heineman received a B.S. degree from Texas Tech University in 1964 and a Ph.D. from the University of North Carolina at Chapel Hill in 1968. He was a research chemist at the Hercules Research Center from 1968 to 1970 before becoming a research associate with Professor Ted Kuwana at Case Western Reserve University and The Ohio State University. He joined the faculty at the University of Cincinnati in 1972 where he is Distinguished Research Professor. Heineman's research interests include biosensors, optically transparent thin-layer electrodes, bioelectrochemistry, thin-layer differential-pulse voltammetry, stripping voltammetry, development of $^{99m}$Tc radiopharmaceuticals, immunoassay by electrochemical techniques, polymer-modified electrodes, and EXAFS spectroelectrochemistry.

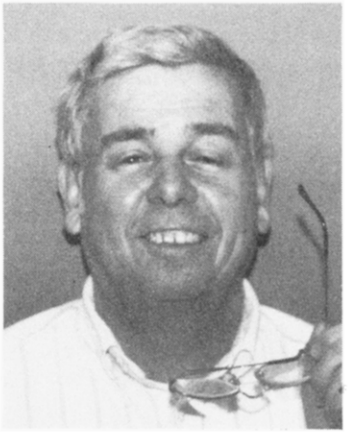

Richard C. Elder was born in Ann Arbor, MI, in 1939. He obtained the undergraduate degree of Honors B.S. in Chemistry in 1961 from St. Louis University. He completed his Ph.D. studies with Professor F. A. Cotton at the Massachusetts Institute of Technology in 1964. After a 1-year postdoctoral stint in Professor Cotton's laboratory at MIT, he was appointed Instructor and then Assistant Professor at the University of Chicago. He came to the University of Cincinnati in 1970 and was promoted to Full Professor in 1978. His research interests include studies of metallodrugs and their metabolites as well as the development of new structural tools using synchrotron X-rays.

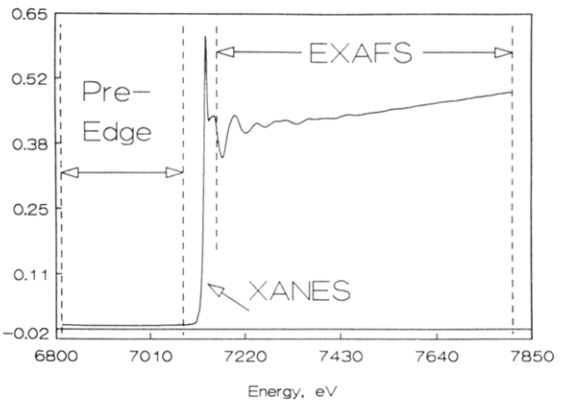


**Figure 1.** Raw X-ray absorption spectrum.

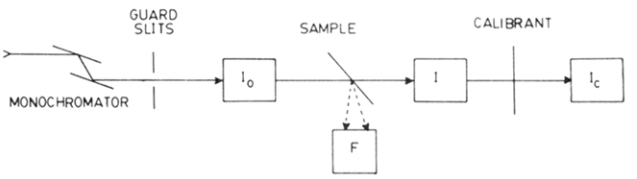


**Figure 2.** Experimental arrangement for simultaneously measuring X-ray transmittance (I), fluorescence (F), and calibration ($I_c$) signals. Reprinted from ref 8; copyright 1985 American Chemical Society.

polymer-modified electrodes, supported catalysts, and thin films. Some examples of ex situ experiments will be discussed for comparison. We begin with a discussion of the experimental techniques and electrochemical cells used and then discuss specific cases.

## II. Experimental Configuration for in Situ X-ray Measurements

The simplest and most direct experimental method to measure EXAFS data utilizes transmission spectroscopy as shown in Figure 2. Ionization chambers are placed in front of and behind the sample in the X-ray beam path in order to measure the intensity of the beam before and after the sample. These detectors can measure the high X-ray fluxes associated with synchrotron radiation sources. The amount of sample used is determined by the absorptivity of the elements comprising the sample. X-ray absorption cross-sections for the elements are available.[7] Ideally, the amount of sample used should give 60–80% transmittance below the absorption edge of interest and 15–30% transmittance at the top of the edge rise.

Fluorescence detection is much more sensitive and can be used for surface studies (i.e., the study of the material that is within a few nanometers of the surface layer). Figure 2 shows the common experimental geometry used by Elder and Heineman in which both transmittance and fluorescence signals are measured simultaneously.[8] The X-rays are first diffracted by a double-crystal monochromator (Si(111) or Si(220)) and

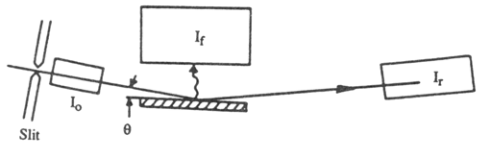


**Figure 3.** Glancing incidence experimental arrangement for simultaneously measuring X-ray fluorescence ($I_f$) and reflectance ($I_r$). Adapted from ref 11.

then passed through a set of slits. The X-ray intensity impinging on and transmitted by the sample (45° off-axis) is measured by the gas-filled ionization chambers labeled $I_o$ and $I_t$. The fluorescence is measured by a Lytle detector[9] positioned at 90° with respect to the beam. A filter assembly is used in front of the $I_f$ detector to remove scattered X-rays.[10] A final ionization chamber is used to obtain an internal calibration of the X-ray energy using a calibrant of known edge energy. Surface studies in this geometry require a very thin film of the sample deposited onto a substrate free from the element under investigation. Even then, Compton and elastic scattering from the substrate can obscure the signal.

If the sample position is adjusted so that the X-ray beam is grazing the surface of the sample, EXAFS measurements of just the surface of the sample can be achieved. At X-ray wavelengths, the index of refraction of materials is slightly less than 1. As a result, when the X-ray beam is at grazing incidence (typically a few millirads), total external reflection will occur.[11] The penetration depth of the X-ray beam under these conditions is approximately 2–4 nm. This configuration has been used to obtain acceptable signal to noise ratios for submonolayer films. A detector in addition to the fluorescence ($I_f$) detector can also be placed in the setup to monitor the reflected X-ray beam as shown in Figure 3. The reflected signal (reflEXAFS) is, however, significantly inferior to the fluorescence signal. There are several difficulties in this experiment that must be appreciated. Since the grazing angle must be less than a few tenths of a degree, the sample surface must be quite flat for this to be possible. In a rough sample, significant portions of the beam will enter at an angle above the critical value and then penetrate deeply into the sample. Another problem is that the scattering efficiency of the element of interest is changing as the X-ray energy is scanned through the absorption edge. This results in a differing penetration depth before total reflection occurs, and thus the EXAFS signal is not all acquired from the same depth. While calculations of interatomic distances are not greatly affected, coordination numbers are and so must be treated with caution.

The above-mentioned techniques are applicable to in situ studies of electrochemical systems. Another detection method, electron yield, has been used in ex situ experiments. Electron yield detectors are surface-sensitive due to the short mean free path of the electrons emitted from the sample. One detector, shown in Figure 4, that measures electrons ejected from a sample can be operated at atmospheric pressure with He gas.[12] This detector utilizes a He-filled ionization chamber in which the sample is used as the photocathode. The X-ray beam impinges the surface of the sample at grazing incidence, causing the emission of electrons. These electrons then impact ionize the helium gas as

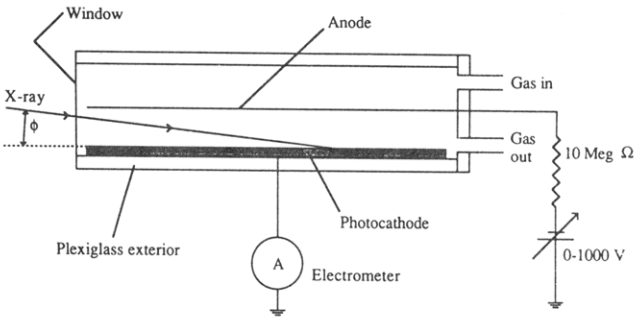


**Figure 4.** Atmospheric pressure electron yield detector utilizing photocathode emissions. Adapted from ref 12.

they travel to the anode, thereby amplifying the signal. This detector weighs higher energy electrons more strongly than lower energy electrons and, consequently, responds primarily to the Auger electrons. The kinetic energy of the photoelectrons and inelastic electrons (Auger or photoelectrons that have suffered inelastic collisions) is too small in most cases to ionize the helium gas, and therefore these electrons are not amplified. The efficiency of this detector was found to be at least 1 order of magnitude better than the grazing incidence fluorescence detector for the low-Z element, copper.[13] However, it requires that the sample be conductive.

In addition to the above methods, EXAFS can be measured in the dispersive mode allowing the acquisition of an EXAFS spectrum in as little as 16 ms,[14] which enables one to perform time-resolved experiments (see section V.A). This technique utilizes a cylindrically bent triangular Si(111) or Si(311) crystal to focus and disperse the X-ray beam onto the sample. Once through the sample, the beam diverges toward a position-sensitive detector. Thus, an entire spectrum can be recorded at once as opposed to step by step data acquisition. The dispersive technique can also be performed by reflection much like the reflEXAFS experiment discussed above. In this experiment the focused and dispersed beam is reflected at grazing incidence off the sample (which is at the focal point) and then diverges toward the position-sensitive detector. The sample surface needs to be "optically perfect"; otherwise, the energy resolution of the beam will be reduced.[15].

## *III. Electrochemical Cells Used in EXAFS Spectroelectrochemistry*[16]

When designing an in situ cell for EXAFS spectroelectrochemical studies, one needs to keep the following points in mind: (1) that complete electrochemical conversion of the material of interest must be achieved, (2) that the diffusional distances and cell resistance should be minimized so that conversion of the material takes place in a reasonable length of time, (3) that enough material to obtain a good EXAFS signal can be incorporated in the cell, and (4) that the cell windows and other components that are in the X-ray beam are transparent to X-rays. Table I compares the transmittances of a variety of cell component materials (in the dimensions typically used in a thin-layer cell).[17] Note that water is a large attenuator. As a result, it is important to use thin-layer cells to keep absorption by the solvent to a minimum. The use of thin-layer cells is also important in fluorescence measurements if an

**TABLE I. Transmittance[a] of EXAFS Spectroelectrochemical Cell Components and Cells[17]**

| energy, keV | 1-mm quartz | $H_2O$ ($\rho$ = 0.997, $\tau$ = 0.25) | Mylar[b] ($C_{11}H_{11}O_5$; $\rho \approx 1.4$, $\tau$ = 0.001 27) | Kapton[c] ($C_{22}H_{10}O_5N_2$; $\rho$ = 1.42, $\tau$ = 0.001 27) | Au[d,e] ($\rho$ = 19.29, $\tau$ = 0.000 33) | RVC C ($\rho$ = 0.048, $\tau$ = 0.25) | RVC[f] cell |
|---|---|---|---|---|---|---|---|
| 6 | <0.001 | 0.00218 | 0.750 | 0.974 | 0.812 | 0.880 | 0.00182 |
| 8 | <0.001 | 0.0760 | 0.886 | 0.992 | 0.852 | 0.948 | 0.0709 |
| 10 | 0.007 | 0.265 | 0.939 | 0.994 | 0.892 | 0.973 | 0.255 |
| 15 | 0.226 | 0.659 | 0.980 | 0.998 | 0.897 | 0.990 | 0.650 |
| 20 | 0.520 | 0.817 | 0.990 | 0.999 | 0.922 | 0.995 | 0.811 |
| 30 | 0.798 | 0.910 | 0.995 | 0.999 | 0.962 | 0.997 | 0.906 |

[a] $I/I_0 = \exp[-\tau\rho\sum_i M_i(\mu/\rho)_i]$, where $\tau$ = thickness (cm), $\rho$ = density (g/cm$^3$), $M_i$ = mass fraction of element $i$, and $(\mu/\rho)_i$ = mass attenuation coefficient of element $i$ (cm$^2$/g). Calculation from ref 7, pp 51–111. [b] Poly(ethylene terephthalate) (Du Pont). [c] Polyimide film (Du Pont). [d] $I/I_0 = 0.8 + 0.2[\exp[-\tau\rho(\mu/\rho)]]$. Gold minigrid has 80% visible transmission. [e] One layer of 100-lpi gold minigrid. [f] RVC cell: $H_2O$ × Kapton$^2$ × RVC.

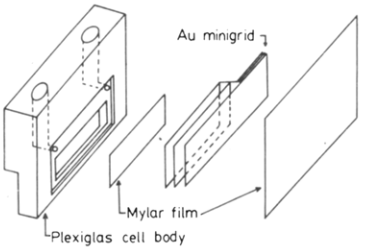


**Figure 5.** Gold minigrid cell for EXAFS spectroelectrochemistry. Reprinted from ref 8; copyright 1985 American Chemical Society.

internal calibrant is being simultaneously measured.

## A. Solution Cells

Typically, solution cells utilize a thin-layer geometry to enable rapid and complete electrolysis. The first solution EXAFS spectroelectrochemical cell was based on an earlier design of an optically transparent thin-layer electrode[18,19] and utilized three pieces of 100 lines/in. (lpi) gold minigrid as the working electrode to minimize diffusional distances (Figure 5).[8] The dimensions of the thin-layer cell were chosen so that all of the ca. 18 × 2 mm cross-sectional area of the available X-ray beam (at SSRL) passed through the working electrode. The minigrid sheets were separated by 0.33 mm with layers of adhesive Teflon tape. Electrical contact was made directly to the minigrids where they extended beyond the cell body. Two access ports were drilled in the top corners of the cell. Each housed a counter and reference electrode and provided a means of filling the cell. The two counter and two reference electrodes were shorted together, respectively. This cell worked well except for the long (ca. 30 min) electrochemical conversion times required due to the $iR$ drop of the cell and the relatively long diffusion distances involved.

A later cell reduced the electrolysis time by utilizing a reticulated vitreous carbon (RVC) electrode.[17] The reduction in the conversion time is important due to the limited time available on a synchrotron beam line. RVC is composed entirely of carbon, which results in less X-ray attenuation and scattering as compared to gold minigrid. The free void volume of RVC accounts for 97% of the total volume. This results in most of the solution being contained inside the electrode and therefore gives a shorter average diffusional path to the electrode surface. The latest version of this cell is shown in Figure 6. The cell was machined from Macor, a ceramic material, for use with nonaqueous solvents.[20] Two reference electrodes were shorted together and

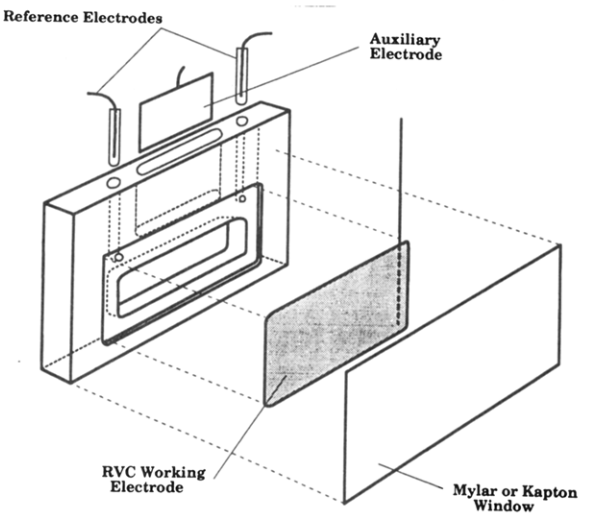


**Figure 6.** Reticulated vitreous carbon electrochemical cell for EXAFS spectroelectrochemistry.[20]

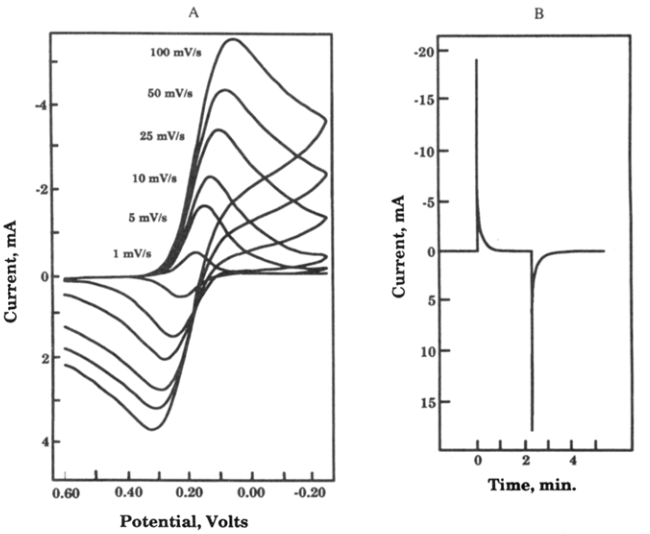


**Figure 7.** (A) Cyclic voltammograms of 1 mM $K_3Fe(CN)_6$–0.5 M $KNO_3$ at different scan rates. (B) Chronoamperometry of 1 mM $K_3F_3(CN)_6$–0.5 M $KNO_3$.

placed in the two filling ports. A large platinum foil was used as th auxiliary electrode in a well above the RVC working electrode. This configuration allows gas bubbles produced on the auxiliary electrode to escape from the cell. The windows were either Kapton (polyimide) tape or Mylar (poly(ethylene terephthalate)) to reduce X-ray attenuation. The electrochemical performance of this cell measured by cyclic voltammetry and chronoamperometry is shown in Figure 7 for a 1 mM $K_3$-

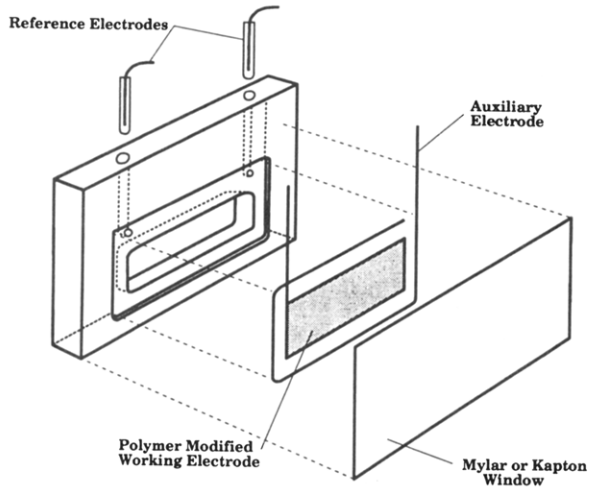


**Figure 8.** Polymer-modified electrode cell for EXAFS spectroelectrochemistry.

$Fe(CN)_6$ solution. The peak separation observed in the cyclic voltammograms (Figure 7A) is greater than the expected value of 0 mV for thin-layer behavior due to the uncompensated $iR$ drop between the RVC and reference electrodes. Note also the short electrolysis times required for this cell in the current vs time plot (Figure 7B).

## B. Polymer Film Cells

The study of polymer-modified electrodes has the advantage that all the material of interest is confined in a film adjacent to the surface of the electrode. Thus, the amount of solution in the X-ray beam can be decreased either by using a thinner solution compartment or removing most of the electrolyte after electrolysis of electroactive species in the polymer film. We studied Nafion (a copolymer of tetrafluoroethylene and perfluoro-4-methyl-3,6-dioxa-7-octenesulfonic acid) films supported on thin graphite working electrodes mounted 45° with respect to the X-ray beam. We measured EXAFS[21] in the cell shown in Figure 8. The working electrode was prepared by spraying several layers of colloidal graphite onto a strip of Mylar. In later work, we have used[20] a thin gold film (300 Å)/Mylar substrate, resulting in better electrochemical properties. The cell was machined from Plexiglas (poly(methyl methacrylate)), and the "back" of the working electrode was placed against the Kapton tape window. This configuration is important for the fluorescence measurement in that it reduces absorptive losses. The incoming X-ray and outgoing fluorescence photons need only penetrate the Kapton window, the Mylar substrate, the gold film, and the Nafion and carbon layer, and not the solution layer, which is by far the most absorbing component. To avoid shorting of the working and auxiliary electrodes, Kapton tape was interleaved between the two electrodes. The holes on the top of the cell were used to fill the cell and mount the two reference electrodes, which were shorted together.

Abruna has studied the EXAFS of electropolymerized ruthenium and osmium vinylbipyridine polymers at grazing incidence in the cell shown in Figure 9.[22,23] This cell was machined from a Teflon (poly(tetrafluoroethene)) cylinder. Contacts for the three electrodes and Teflon fittings for the injection of electrolyte were positioned as shown. The working electrode was

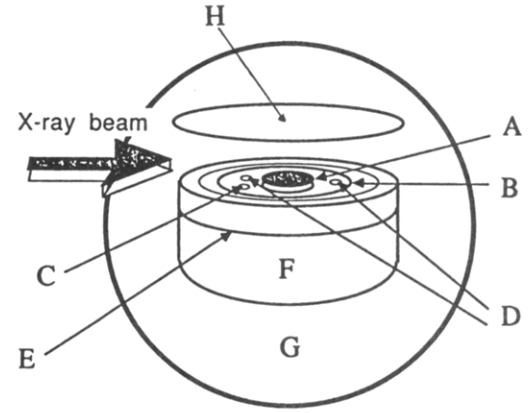


**Figure 9.** Electrochemical cell for surface EXAFS of chemically modified electrodes: (A) Pt-disk working electrode; (B) Pt auxiliary electrode; (C) reference electrode port; (D) electrolyte ports; (E) viton O-ring; (F) Teflon cell body; (G) Huber 410 goniometer; (H) Tezfel film window. Adapted from ref 23.

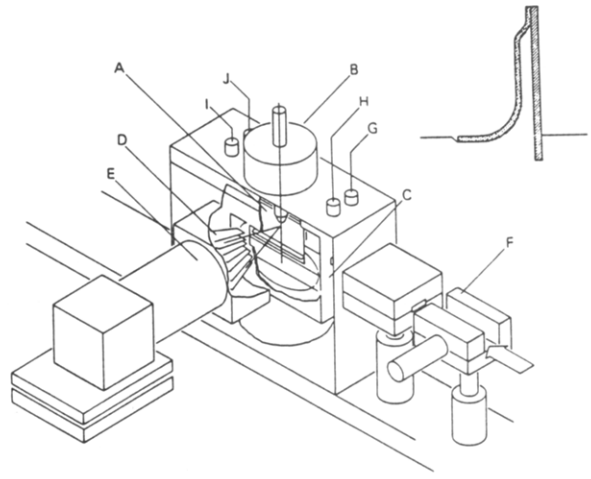


**Figure 10.** Electrochemical cell for surface EXAFS of thin metal films: (A) Lexan sample holder; (B) rotating stage; (C) Lexan cell; (D) Sollar slits; (E) high-purity germanium solid state detector; (F) slits; (G) port for reference electrode; (H) port for helium; (I) auxiliary electrode; (J) electrolyte port. Inset: the electrode in thin film configuration. Reprinted from ref 25; copyright 1987 American Chemical Society.

placed on top of the cell and covered with a thin Tezfel film, which allowed only a thin layer ($\sim$20 $\mu$m) of electrolyte to remain in contact with the electrode, reducing the attenuation of the X-ray beam by solution. The cell was placed in a Plexiglas box with Kapton windows and flushed with helium. The entire assembly was mounted on a goniometer stage, allowing for fine positioning.

Tourillon et al. used a two electrode cell consisting of a platinum wire working electrode covered by an electropolymerized thiophene polymer and a platinum auxiliary electrode.[24] The cell solution compartment was composed of a 2–3-mm-thick Teflon ring covered with two Kapton windows.

## C. Metal, Passive, and Oxide Film Cells

EXAFS spectroelectrochemical studies of thin metal films on noble metals or passive/oxide films on metal electrodes have the same advantage as those of polymer films: the electrolyte layer can be reduced, resulting in less attenuation of the X-ray beam.

Researchers at IBM have used the cell shown in Figure 10 to study thin metal films underpotentially

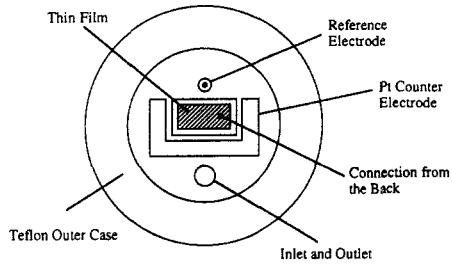


**Figure 11.** "Piston" arrangement electrochemical cell for surface EXAFS measurements. Adapted from ref 26.

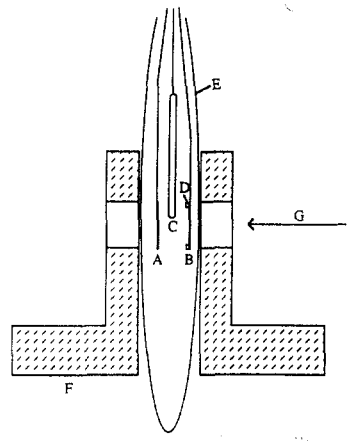


**Figure 12.** "Bag cell" for thin-layer EXAFS spectroelectrochemistry: (A) iron film working electrode; (B) gold auxiliary electrode; (C) Pd–H reference electrode; (D) Teflon spacer; (E) polyethylene bag; (F) vise assembly. Adapted from refs 27 and 28.

deposited onto noble-metal film electrodes.[25] The working electrode was mounted on a Lexan holder, which was attached to a rotating stage allowing for the alignment of the sample. The cell was constructed of Lexan and equipped with Mylar windows. Ag/AgCl was used for the reference electrode and platinum wire for the auxiliary electrode. During data collection, the level of electrolyte was reduced so that it was below the X-ray beam. A thin layer of electrolyte remained between the electrode and the Mylar window, which was attached to the top of the electrode by capillary action (see inset in Figure 10). When deposition was performed, the electrolyte level was raised, which caused the Mylar film to float and exposed the electrode to the bulk electrolyte. This cell has the advantage that deposition is performed with the electrode exposed to bulk electrolyte, whereas during data collection the cell is in a thin-layer arrangement.

Long et al. have used a similar concept in their cell shown in Figure 11.[26] In this case, the inside of the cell was mounted on a piston that was withdrawn from the window into the bulk electrolyte in order to perform the electrolysis, and then after electrolysis when the current had dropped to a small amount, it was moved back to be nearly in contact with the window. Potential control was maintained throughout this process. All three electrodes were embedded in an inert epoxy so that they were coplanar. The working electrode was prepared by deposition of the metal sample on the surface of a glass slide.

Hoffman has developed two unique electrochemical cells for the study of electrochemical interfaces.[27,28] The first is the "bag cell" shown in Figure 12. The sample was deposited onto a gold/Melinex substrate, which was

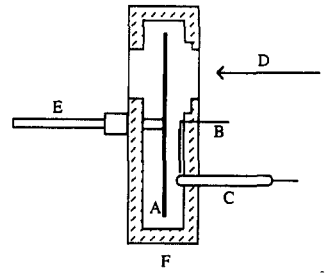


**Figure 13.** Rotating disk electrochemical cell: (A) rotating disk working electrode; (B) gold foil auxiliary electrode; (C) Pd–H reference electrode; (D) X-ray beam; (E) rotating shaft assembly. Adapted from refs 27 and 28.

used as the working electrode. The auxiliary electrode, a piece of gold foil, was separated from the working electrode by a Teflon spacer. Palladium with adsorbed hydrogen served as the reference electrode. When electrolysis was taking place, the bag was loose to allow an ample volume of electrolyte around the electrodes. After the electrolysis was complete, the auxiliary electrode was raised out of the X-ray beam and the cell width was reduced by pushing together the walls of the bag. The second cell utilizes a large rotating disk working electrode (Figure 13) in which only half is in contact with the electrolyte. Thus, the lower half is under potential control in the electrolyte, and the upper half is exposed to a helium atmosphere where the XAS measurement is made. Whether potential control is maintained in the upper half of the electrode is not clear.

Bosio et al. have developed two cells for reflEXAFS studies.[29] One uses a piston similar to that in Long's cell. The other, shown in Figure 14, is a three-electrode cell in which the sample working electrode is on the bottom of the cell. The X-ray beam enters in the front Mylar window, reflects off the working electrode, and exits through the back window.

McBreen et al.[30] have studied the oxidation of $Ni(OH)_2$ in a two-electrode transmission cell shown in Figure 15. The preparation of the working electrode is described in section VI.B.2. The cell is comprised of two acrylic end pieces, each with an acrylic window 0.75 mm thick. The internal components of the cell include a nickel oxide working electrode and a 0.125-mm Grafoil counter electrode separated by three layers of filter paper that, soaked with electrolyte, provide a current path and keep the electrodes from shorting. Each component is mounted in a PTFE gasket, and the assembly is bolted together.

As one can see, there are several quite different electrochemical cells that have been successfully utilized to obtain in situ structural information using EXAFS. They all are able to achieve complete electrochemical conversion of the material of interest in sufficient concentration or amount to yield an adequate EXAFS signal. They all either are thin-layer cells or can be made into thin-layer cells by removing electrolyte after the electrolysis. Another feature is that most of the cells provide potentiostatic control throughout the experiment.

## *IV. EXAFS Spectroelectrochemisty of Solutions*

Much electrochemistry is performed at submillimolar concentrations. These low concentrations present a

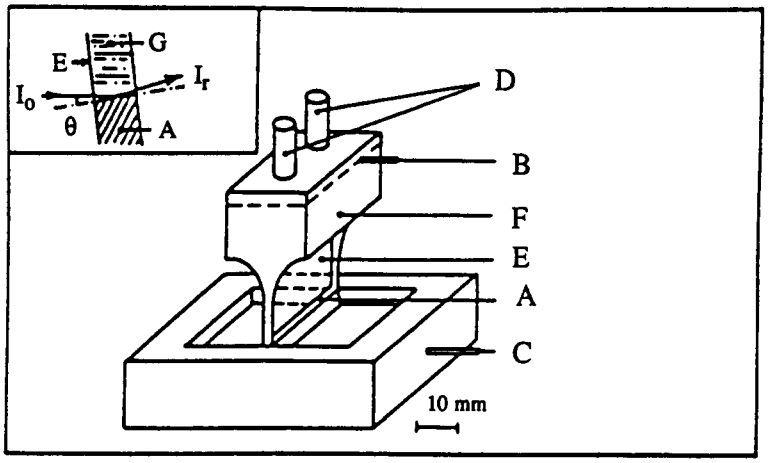


**Figure 14.** Electrochemical cell for EXAFS studies of thin films: (A) sample; (B) electrical connection to Pt grid auxiliary electrode; (C) electrical connection to the working electrode; (D) electrolyte inlet and outlet; (E) Mylar windows; (F) plastic cell; (G) electrolyte. Adapted from ref 29.

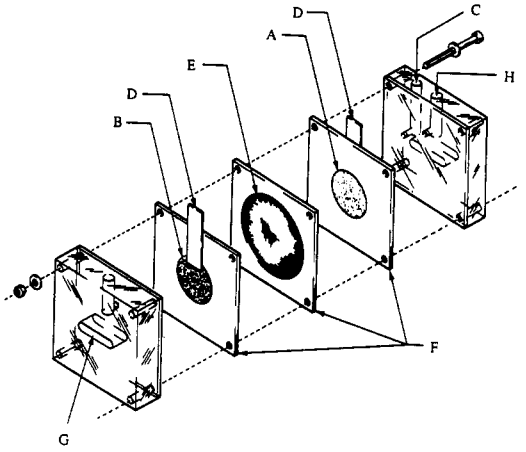


**Figure 15.** Transmission electrochemical cell for the study of $Ni(OH)_2$ electrodes: (A) nickel oxide working electrode; (B) grafoil auxiliary electrode; (C) reference electrode; (D) nickel current collector; (E) separator; (F) gaskets; (G) window; (H) electrolyte port. Adapted from ref 30.

problem for EXAFS measurements due to the weak signal obtained with dilute samples. In order to determine a working concentration range for the EXAFS spectroelectrochemistry experiment, several concentrations of $[Ru(NH_3)_6]Cl_3$ were measured in a RVC cell similar to the one shown in Figure 6.[17] The effect on signal to noise ratio as a function of concentration is demonstrated by the spectra obtained from 100, 10, and 1 mM solutions of $[Ru(NH_3)_6]Cl_3$ as shown in Figure 16. The deterioration of the transmission data as concentration decreases is much more pronounced than it is for the fluorescence data. All three concentrations yield similar Fourier transforms (of the fluorescence data) that show one major peak corresponding to the Ru–N absorber–scatterer pair. The Fourier-filtered (back-transformation of the peak) data for the three concentrations are nearly indistinguishable from each other. The curve-fitting results agree within ±0.02 Å of the crystallographic bond distance for Ru–N and were not affected significantly as the concentration was lowered. From these results, it appears that ruthenium solutions of $10^{-4}$ M could readily be measured by EXAFS. First-row transition elements require a higher concentration, ca. $10^{-3}$ M, as a result of lower fluorescence yields and higher background scatter.

The ability to control precisely the potential of an electrochemical cell and thus the ratio of the oxidized to reduced species can be important in certain situations.[31,32] Precise potential control of the RVC cell shown in Figure 6 is demonstrated with spectra of cobalt sepulchrate at a series of applied potentials.[17] In this experiment the potential applied to the cell was incrementally varied to produce Nernstian Co(III)/Co(II) ratios. The cobalt absorption edge in Figure 17 can be seen to shift to lower energy with each more negative potential step. Four isosbestic points were observed, demonstrating the smooth conversion of the Co(III) to the Co(II) species in the EXAFS spectroelectrochemical cell.

The determination of solution metal–ligand bond distances as a function of oxidation state is necessary for the calculation of electron transfer rates from Marcus–Hush theory.[33] The use of bond distances determined by single-crystal X-ray diffraction causes problems since for a given oxidation state metal–ligand distances vary considerably. Not only are different distances found for a given crystal, but also more widely varying distances are found as counter ions and degree of hydration are varied. Clearly the answer is to determine bond distances in solution. An example of this problem is illustrated with the ferri/ferrocyanide couple. X-ray spectra of a solution of ferricyanide, Fe(III), and in situ electrogenerated ferrocyanide, Fe(II), have been measured by fluorescence detection at 45° with respect to the X-ray beam.[8,34] The concentration of Fe(III) was 10 mM, and the supporting electrolyte was 1 M lithium acetate. The supporting electrolyte is composed of low atomic numbered elements to allow for high X-ray transmittance and is in high concentration to reduce cell resistance. The relatively high Fe(III) concentration was used in order to obtain a good EXAFS signal (vide supra). This experiment was performed in the gold minigrid solution cell shown in Figure 5. The solution could be 95% reduced when the cell potential was stepped to −200 mV vs Ag/AgCl for 30 min and reoxidized in 20 min at a potential of 500 mV.

The Fourier transforms of the EXAFS spectra exhibited two major peaks corresponding to carbon and nitrogen back-scatterers. The nitrogen atom, which is in the second shell from the iron-absorbing center, contributes significantly more back-scattering than

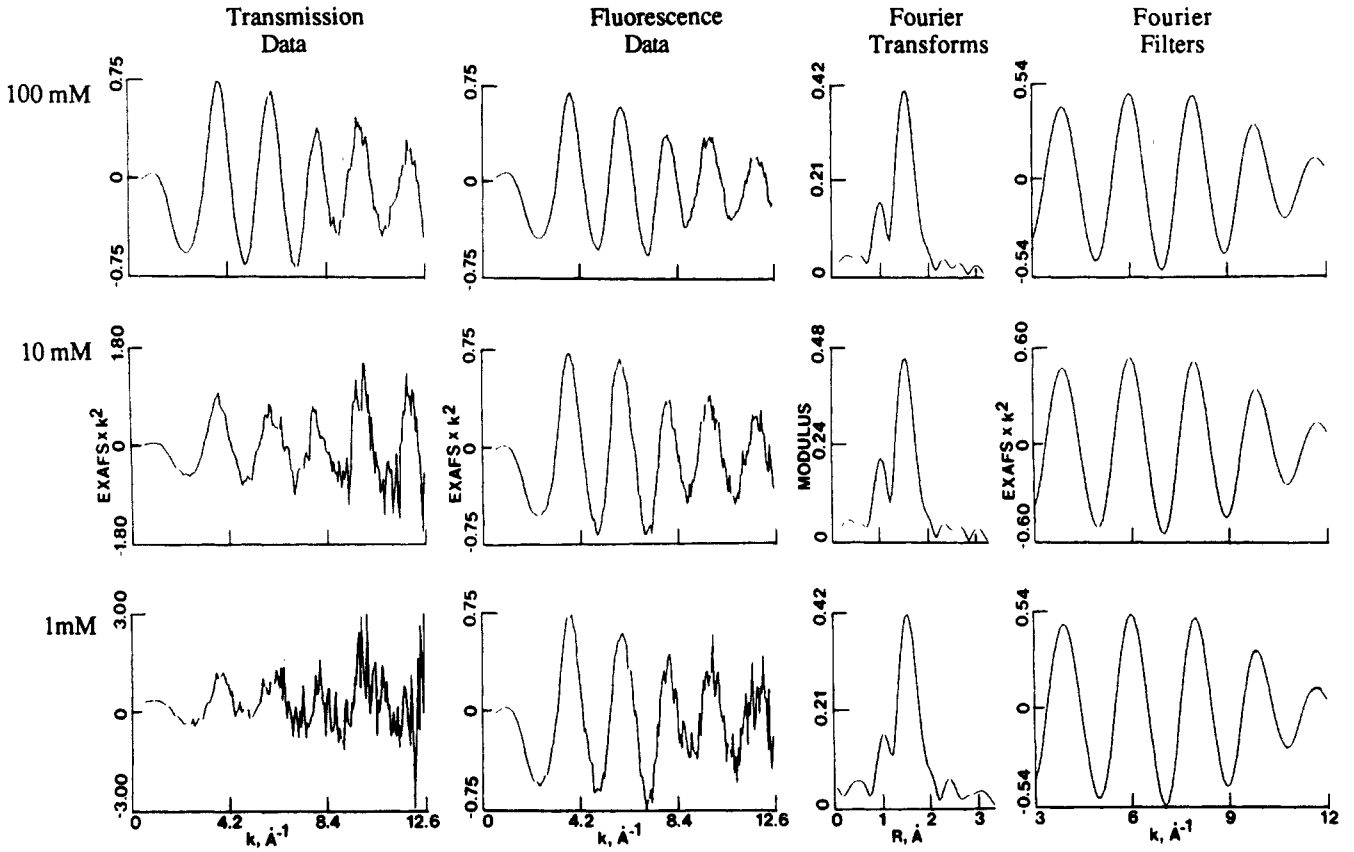


**Figure 16.** EXAFS spectra of $Ru(NH_3)_3$ in 1 M sodium acetate at different concentrations. Reprinted from ref 17; copyright 1986 American Chemical Society.

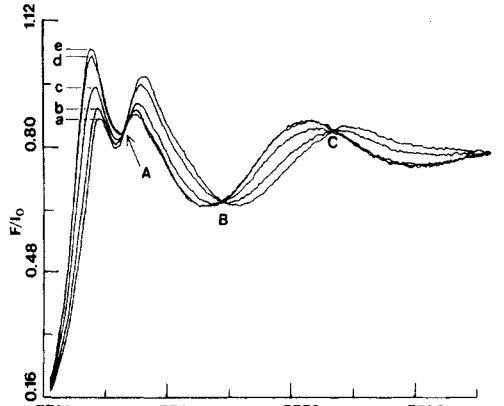


**Figure 17.** XAS of 10 mM cobalt sepulchrate in 1 M sodium acetate. Applied potentials: (a) −0.30 V, (b) −0.58 V, (c) −0.60 V, (d) −0.62 V (e) −0.80 V vs Ag/AgCl. Reprinted from ref 17; copyright 1986 American Chemical Society.

might be expected as a result of the collinearity effect.[35] The Fe–C bond distance was found to increase by 0.03 Å upon reduction from Fe(III) to Fe(II). The increase was invariant, whether an Fe(III) or Fe(II) solid model was used, although the absolute distances were shifted to 0.03 Å less when Fe(II) was used as the model. The EXAFS results for the solids containing Fe(III) and Fe(II) were consistent with the solution EXAFS. The error in the bond distances was estimated to be 0.01 Å. The EXAFS results were found to be inconsistent with the grand averages of all Fe(II) and all Fe(III) structures, which suggest that the Fe(II)–C distance is 0.01 Å less than that for Fe(III)–C. It is not clear why the discrepancy, which is barely significant, occurs. It may be that the grand averages are strongly biased by one or more disordered structures or the tendency of these materials toward polytypism.[36] Perhaps this discrepancy accurately reflects a difference between the solution and the solid state.

Redox-active biological samples in solution have additional problems. These materials have been shown, upon exposure to X-ray radiation, to be reduced by hydrated electrons produced by the interaction of the X-rays with water.[37] Dewald et al.[17] observed a 40% reduction of a 10 mM solution of horse heart cytochrome *c* after 6 h of X-ray illumination in the absence of potential control. This X-ray-induced reduction of a solution species demonstrates the need for in situ potential control during the EXAFS experiment. Cytochromes are bioinorganic complexes displaying a wide variety of redox potentials not due to a difference in their ligating atoms but possibly differences in their iron–ligand bond length or orientation. Korszun et al.[38] studied a series of cytochromes *c* exhibiting a significant range of reduction potentials with EXAFS and observed no average Fe–ligand bond distance difference greater than 0.03 Å. In this work the complexes were chemically oxidized and reduced. Dewald et al. performed a similar experiment on 10 mM horse heart cytochrome *c* utilizing their in situ EXAFS electrochemical cell. Since, under the conditions of this experiment, cytochrome *c* is reduced slowly at a metal electrode, an organic mediator, 2,6-dichlorophenol–indophenol, was added. This material was rapidly reduced at the electrode and in turn reacted rapidly with the protein. The Fourier transform of the EXAFS yields one main peak corresponding to both the Fe–N and Fe–S interactions. Curve fitting of these results by empirical phase and amplitude functions derived from solid cytochrome *c*

indicated no significant bond length difference between the two oxidation states.

## V. EXAFS Spectroelectrochemistry of Polymeric and Catalytic Systems

### A. Polythiophene

Conducting polymers have received considerable attention as a result of their impressive electrical conductivities and their potential application to a variety of devices. Polythiophene and its derivatives show the highest promise due to their excellent moisture and oxygen stability.[39] Films of polythiophene can be electrochemically deposited on electrodes by application of a positive potential. The resulting polymer is in the so-called doped state (electron density has been removed from the "conduction band", resulting in a partially filled band that allows the polymer to be conductive) and can be reversibly reduced to its undoped state electrochemically. The thickness of the film can be controlled by varying the time of deposition. The structural aspects of the growth of these films are important to understand since most applications depend on charge transfer that occurs at the metal–polymer interface.

Tourillon and co-workers have used XANES and EXAFS to determine the geometric and electronic structure of poly(3-methylthiophene) (PMeT) electrochemically deposited at 1.8 V vs SCE onto platinum electrodes.[40-42] The structural conformation of the monomer was found to be retained upon polymerization. The orientation of the thiophene rings in the doped state varied with thickness. The first layer lies flat on the platinum surface, and additional layers are randomly oriented. The undoped film remained oriented flat throughout film growth. In a comparison of the XANES spectra of the doped and undoped films, the authors noted that the doping process removes an electron from the $\pi$ band, which extends the $\pi$ and $\pi^*$ bands to the Fermi level, resulting in the metal-like properties of the doped film.[43] Sulfur EXAFS spectra have demonstrated that the S–C bond length does not change when the polymer is doped and that the sulfur interacts with the counter ion in the doped state. The effect of the charge and size of the counter ion on the conductivity of the polymer was reported by Tourillon and co-workers.[44] In addition, EXAFS was used to determine the coordination environment around the metal complex anions studied.

Similar results were found for polyselenophene.[45] This polymer has the advantage over polythiophene in that in situ studies can be performed as a result of the higher energy absorption edge of selenium. XANES studies indicated that the electron removed from the polymer during oxidative doping comes from the analogous $\pi$ band as in the thiophene case. This material has similar metal-like properties. The selenium EXAFS from the undoped and doped materials were Fourier transformed and showed significant differences. The undoped form showed two selenium–carbon interactions to the $\alpha$- and $\beta$-carbons of the selenophene ring. In the doped state, there was little indication of the $\beta$-carbon and a new peak for a longer distance interaction was observed. These observations were accounted for by postulating a rearrangement of the polymer chains on doping such that an inter- or intrachain Se–C interaction interfered with and weakened the Se–$C_\beta$ signal, and at the same time, the Se–Se interaction became more rigidly fixed.

Earlier work by Tourillon involved EXAFS studies of copper metal clusters in PMeT.[14,24,46,47] Studies showed the catalytic activity of these matrices depended strongly on both the location and size of the metal clusters.[48] EXAFS offered an excellent way in which to study in situ the incorporation of copper into PMeT, which was found to occur in a stepwise fashion. PMeT was electrochemically deposited onto a platinum wire at 1.35 V vs SCE in the presence of $SO_3CF_3^-$ ion. The resulting conductive polymer was placed in a 3-mm-thick, two-electrode cell composed of a Teflon ring covered by two Kapton windows and filled with cupric chloride solution. The X-ray beam was focused by a bent Si(111) crystal on the polymer close to the platinum wire, and the energy-dispersed, transmitted beam was detected by a photodiode array made of 1024 sensing elements having a resolution of 2.5 eV. A time-resolved investigation of the incorporation of the copper indicated that three steps were involved. First, upon application of a −2.0-V potential to the polymer in the presence of concentrated $CuCl_2$, a rapid conversion from $Cu^{2+}$ to $Cu^+$ was observed by XANES. The $Cu^+$ was said to be complexed by oxygens from the $SO_3CF_3^-$ ions at a distance of 1.91 Å on the basis of EXAFS data. There seems to be no reason why the oxygen could not come from water molecules instead. The Cu–O distance falls between those for $Cu_2O$ and CuO, which are 1.85 and 1.95 Å, respectively, and perhaps this rather short Cu–O distance argues for binding to the charged sulfonate. The second step involved the coordination of the $Cu^+$ to sulfur from the PMeT. In the final step, the $Cu^+$ was reduced to copper metal clusters having (111) plateletlike structures located in the polymer fibers. The incorporation of copper is fully reversible: application of a +1.0-V bias to the cell causes the copper metal to be oxidized to aqueous $Cu^{2+}$.

In dilute solutions ($1 \times 10^{-2}$ M), the reduction of the polymer to a neutral, low-conductivity state took place instead of copper incorporation. Since the polymer behaved like an insulator, the $Cu^{2+}$ ions were not reduced in the polymer fibers, but migrated inside the PMeT and deposited onto the platinum wire.

These results demonstrate the utility of XANES and EXAFS to follow the in situ electrochemical deposition of an organic polymer film and incorporation of a metal into such a film. Insight into the orientation of the polymer film on the electrode surface was obtained in addition to the steps involved in the incorporation of copper into the polymer film. The use of energy-dispersive EXAFS measurements is especially important here. The entire spectrum can be recorded within a few seconds after a potential step is applied, and thus it is possible to follow changes taking place over relatively short time intervals.

### B. Ion-Exchange Polymers

The incorporation of a metal ion or complex into a polymer coating on an electrode provides a means to vary the electrochemical behavior of the electrode.[49] There have been several studies on the redox chemistry

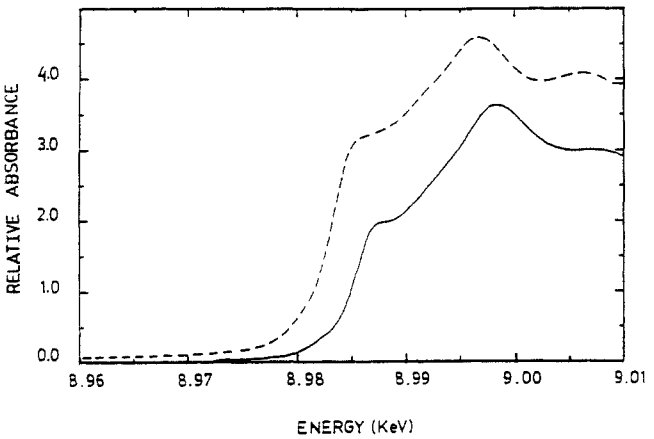


**Figure 18.** Comparison of the XANES spectra of $Cu(dmp)_2NO_3$ solid (---) and the Nafion polymer modified electrode species (—). Adapted from ref 21.

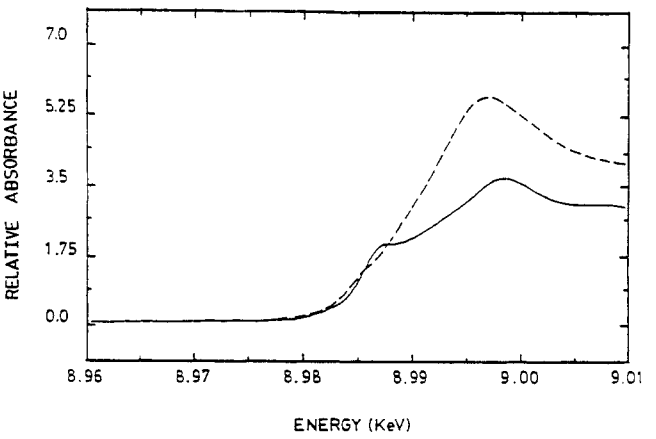


**Figure 19.** Comparison of $Cu(dmp)_2NO_3$ in a Nafion polymer modified electrode (—) and the oxidized form (---). Adapted from ref 21.

of such systems; however, little has been done to characterize the structure of the metal ions or complexes in these films. Elder, Heineman, and co-workers have used fluorescence EXAFS to probe the structures of transition-metal complexes incorporated into bulk ion-exchange polymer membranes immobilized on electrode surfaces. In these experiments, an electrical potential is applied to the polymer-modified electrode to generate and maintain the metal complex in a particular oxidation state while the X-ray absorption spectrum is recorded. Two polymer systems studied by this technique are discussed below.

Nafion is a perfluorinated polymer having sulfonate groups in which the associated proton can be exchanged for other cations. In this work,[20,21] the copper(I) complex bis(2,9-dimethyl-1,10-phenanthroline)copper(I) tetrafluoroborate, $[(Cu(dmp)_2]BF_4$, was exchanged into the Nafion polymer. The hydrophobicity of this copper complex should increase the extraction or partition coefficient[50] and thus increase the amount of copper in the film and the EXAFS signal. This complex was chosen due to its known coordination expansion from 4 to 5 when oxidized to its 2+ state. This system provided an excellent test case for the EXAFS spectroelectrochemistry experiment.

The electrochemical cell used for this study is shown in Figure 8. The working electrode was prepared by spraying several layers of colloidal graphite onto a strip of Mylar. Electrical contact to the film was by silver paint. The Nafion solution was applied to the electrode surface and allowed to dry. The electrode was then placed in a 1 mM solution of the copper(I) complex and allowed to soak overnight.

X-ray spectra were measured at open circuit corresponding to the copper(I) species and at 1.2 V vs Ag/AgCl corresponding to the copper(II) species. X-ray spectra were also measured on solid $[Cu(dmp)_2]BF_4$. Comparison of the edge spectra of the solid and polymer-incorporated $[Cu(dmp)_2]BF_4$ (shown in Figure 18) shows them to be nearly superimposable, indicating that the copper species present in the Nafion prior to electrolysis has the same pseudotetrahedral structure found in the solid state. There was a significant difference between edge spectra of the Nafion-incorporated copper(I) and copper(II) oxidation states as shown in Figure 19. The pronounced shoulder at 8986 eV is nearly missing in the oxidized species, and the maximum has shifted from 8997.7 to 8996.5 eV. The near-edge spectrum provides evidence of the exhaustive in situ oxidation of the starting Cu(I) complex.

Curve fitting of the filtered EXAFS data of the copper(II) complex was accomplished by using empirical parameters derived from the copper(I) complex obtained by setting the copper(I) bond distance equal to 2.06 Å and the coordination number equal to 4. This resulted in a bond length of 2.02 Å and a coordination number of 5 for the copper(II) species. This "extra" fifth ligand is most likely an oxygen either from the sulfonate group on the Nafion or from water present in the polymer film. The inability of the refinement procedure to distinguish adjacent elements in the periodic table leads to the successful modeling of the four nitrogens and one oxygen system by five nitrogens. Subsequent experiments demonstrated similar results for the in situ bulk solution EXAFS spectroelectrochemistry of $[Cu(dmp)_2]BF_4$. This change in structure was found to be reversible in solution as well as in Nafion.

This study demonstrated that in situ fluorescence EXAFS could be used to follow changes in the structure of a metal complex incorporated in an ion-exchange polymer such as Nafion.

### C. Poly(vinylbipyridine)

Abruna and co-workers have recently studied the structure of electropolymerized films of $[M(v\text{-}bpy)_3]^{2+}$ (v-bpy = 4-vinyl-4′-methyl-2,2′-bipyridine) where M = Ru and Os and $[Os(phen)(bpy)_2]^{2+}$ (phen = 4-methyl-1,10-phenanthroline) on platinum electrodes as a function of surface coverage and oxidation state.[22,23,51] The electropolymerization of the complex (0.1–0.5 mM) was carried out in acetonitrile and 0.1 M tetrabutylammonium perchlorate supporting electrolyte in a standard three-compartment electrochemical cell.[52] The modified electrode was then transferred to the EXAFS electrochemical cell (Figure 9) and filled with pure electrolyte. Samples with 1, 5, 12, 25, and 50 monolayers were produced. The EXAFS experiments were performed at grazing incidence, and the X-ray fluorescence was measured with a Si(Li) solid state detector. A monolayer of the polymer contains approximately $5 \times 10^{13}$ atoms/cm$^2$ of metal, which corresponds to about 5% of the metal that would occur in a metal monolayer.

EXAFS of the reduced form of the film was measured at a potential of 0.0 V vs silver wire. The potential was then stepped 300 mV past the oxidation wave to 1.6 V for the ruthenium and 1.1 V for the osmium complexes and held for 5 min to ensure complete conversion to the oxidized form of the film before measurement of the X-ray spectrum.

A distinct ruthenium absorption edge was observed for an electrode having as little as one monolayer of polymer; however, only the first oscillation in the EXAFS region could be discerned due to noise as a result of the small amount of sample and the rapid decrease in back-scattering amplitude for low-Z scatterers. Increased coverage yielded better signal to noise ratios. Curve fitting of the EXAFS data using theoretical amplitude and phase functions yielded bond lengths of 1.9, 2.0, and 2.1 Å for 1, 5, and 50 monolayer films, respectively, all of which had a coordination number of about 6.[22] No significance was placed on the trend in bond length, although the values were stated to correlate very well with crystal structure values of six nitrogens at 2.056 Å.[53] The near-edge spectra were also very similar for the polymer films as well as for the monomeric parent compounds, which was taken to indicate that no significant changes in geometry occur when the complexes are electropolymerized onto an electrode surface. Identical results were obtained for electrodes biased at 0.0 V and at open circuit.

When the electrode was stepped to oxidize the polymer the resulting spectra were virtually unchanged except for a shift in the absorption edge to higher energy by 2 eV. This is consistent with the formation of the $M^{3+}$ centers. The similarity of the spectral features between the two oxidation states is not surprising since the bond length is expected to change by 0.04 Å or less.

Abruna et al. also compared the near-edge features of $[Os(v\text{-}bpy)_3]^{2+}$ and $[Os(phen)(bpy)_2]^{2+}$. They noted that there was a difference in the edge positions and area under the first peak (white line). These differences were attributed to the higher $\pi$ acidity of the phen relative to the bpy ligand, which results in a higher degree of $\pi$ back-bonding and removal of electron density from the osmium, shifting the $[Os(phen)(bpy)_2]^{2+}$ to higher energy.

These experiments are clearly at the limit of what is possible. While it seems likely that the monolayer electropolymerized film contains the six-coordinate ruthenium starting complex intact, the evidence here is not compelling. A bond length of 1.9 Å is far from the expected value and a coordination number of "about 6" could probably be anywhere from 4 to 8. Although the edge rise can be seen for the monolayer, the EXAFS cannot be seen and much less can meaningful distances or coordination numbers be extracted.

## D. Supported Catalysts

The following discussion concerns the use of X-ray spectroscopy to follow changes in the structure and composition of supported catalysts as a function of exposure to oxygen, hydrogen, or vacuum atmospheres. This discussion is not intended to be comprehensive but rather to cite a few examples for comparison to the electrochemical experiments due to the similarity between surface gas-phase reactions and redox reactions at thin film electrodes.

The oxidation and reduction by oxygen and hydrogen, respectively, of a Co–Rh catalyst supported on $SiO_2$ was studied in situ.[54] EXAFS spectra were recorded after the passivated catalyst had been reduced at 673 K under hydrogen and when it was exposed to oxygen at room temperature. The spectra were compared to Co–Rh alloy that was also exposed to the same conditions. The Fourier transforms of the Rh EXAFS data for the reduced catalyst and the alloy both display two similar peaks at 1.9 and 2.4 Å corresponding to Rh–Co and Rh–Rh back-scattering, indicating that the reduction process produces alloyed Co–Rh particles. The relative intensity of the peaks for the two materials is different. The Rh–Co peak in the catalyst is smaller and the Rh–Rh peak larger than the corresponding alloy peaks, suggesting that the rhodium atoms are surrounded by more rhodium atoms than cobalt atoms in the catalyst. Upon exposure to oxygen, the Co–Rh catalyst's Rh EXAFS is slightly changed; however, the Co K-edge EXAFS changes drastically. The Co EXAFS spectrum was characteristic of Co–O coordination. From these data, the authors concluded that two phases were formed during the reduction process, one rich in rhodium that comprised the inside of the particles and a cobalt-rich phase on the surface. This explains the change in the cobalt EXAFS spectra upon oxygen adsorption.

The in situ reduction of Rh supported on $TiO_2$ has been investigated at different temperatures by XANES.[55] In this work, evidence from XANES spectroscopy for the formation of a Rh–Ti species was observed when the catalyst was reduced at temperatures greater than 623 K. The spectrum of the catalyst was compared to those of Rh metal and the intermetallic compounds RhTi and $Rh_3Ti$.

Another example of an in situ study of the oxidation and reduction of a catalyst by oxygen and hydrogen is provided by Koningsberger et al.[56] In this work, a passivated iridium catalyst supported on $\gamma$-$Al_2O_3$ was reduced under hydrogen at 473 K for 1 h in an in situ reactor. X-ray spectra were also measured on the sample after evacuation at 623 K for 2 h after adsorption of oxygen at 7 K and warming under oxygen to 100 K. All spectra were measured at 77 K. The results of the EXAFS experiments were interpreted by analysis of the raw EXAFS data and their Fourier transforms. The reduced form of the catalyst was comprised of highly dispersed metal particles. After evacuation, the amplitude of the EXAFS oscillations was damped at high K values, suggesting a larger degree of disorder in the metal particles. A contraction of the Ir–Ir distance was also observed. Oxygen adsorption at 77 K alters the low-K part of the EXAFS spectrum, which is most likely due to the addition of oxygen nearest neighbors. When the catalyst was heated under oxygen, the frequency of the EXAFS oscillations decreased and the signal was damped to a greater extent, which further supports the conclusion of the formation of oxygen nearest neighbors.

EXAFS has also been used to study catalysts supported in zeolites. An example of this is a study of the decomposition of $Pd(NH_3)_4^+$ exchanged into zeolite X.[57] The X-ray measurements in this case were performed ex situ. EXAFS indicated that the structure of the complex was unchanged as a result of incorporation into

the zeolite and that it was randomly oriented, which was supported by the lack of outer-shell scattering. When the zeolite was heated under vacuum at a temperature above that for ammonia evolution, the resulting EXAFS appeared quite similar to that of the starting material. The authors reasonably postulate that some of the amine ligands have been replaced by oxygens in the zeolite framework. In general, elements of adjacent atomic number have too similar phases and amplitudes as back-scatterers for them to be distinguished by EXAFS. Palladium metal was observed when the zeolite was heated to 623 K. Prolonged heating produced particles 70–90 Å in size. The palladium is believed to be reduced by an autoreduction reaction by remaining ammonia in the zeolite.[58] When the above experiment was performed in air, similar results were obtained up to 523 K. However, further heating did not produce palladium metal; instead, the palladium remained coordinated to the zeolite oxygen sites.

These experiments demonstrate the utility of the EXAFS experiment to follow not only chemical redox processes but chemical decomposition reactions both in situ and ex situ. They are not without some confusion, however. The authors show a Fourier transform $[Pd(NH_3)_4]^{2+}$ and attribute the major peaks to the four amines and additional water molecules. Clearly there are no bound water molecules in the solid, and it seems highly unlikely that in solution any loosley bound water would serve as an effective back-scatterer. This is compounded by the fit of the zeolite-exchanged palladium, which gives a coordination number of 6.5, a most unusual value, considering the normal preference for 4.0.

## *VI. EXAFS Spectroelectrochemistry of Metal, Passive, and Oxide Films*

### A. Passivation of Iron

Many studies of the passivation of iron metal in various solutions have been reported. There is considerable controversy concerning the chemical nature of the films and their structures. In general, passive films are composed of hydrated oxides of the elements in the metals or alloys placed in a "passivating solution". As a result of the degree of hydration involved, it is believed that the structure of the passive film changes upon removal from the passivation solution. Thus, it is essential to perform the structural characterization in situ. Surface EXAFS has proven to be an invaluable means to study the structure of these films. Other techniques require vacuum conditions that are believed to alter the film structure by drying it and causing crystallization.

Hoffman[4] has written a lucid review that considers in detail the experimental difficulties encountered in studying passivated films. The principal problem is that the X-ray-absorbing atoms of the passivated layer are the same element as the substrate and any signal is in general the superposition of that from the bulk material and the passivated layer. Two basic approaches may be followed. First, the substrate may be made so thin that on passivation all of it is converted, or second, a technique that only probes a few atomic layers below the surface may be used.

Long and co-workers studied the EXAFS of iron

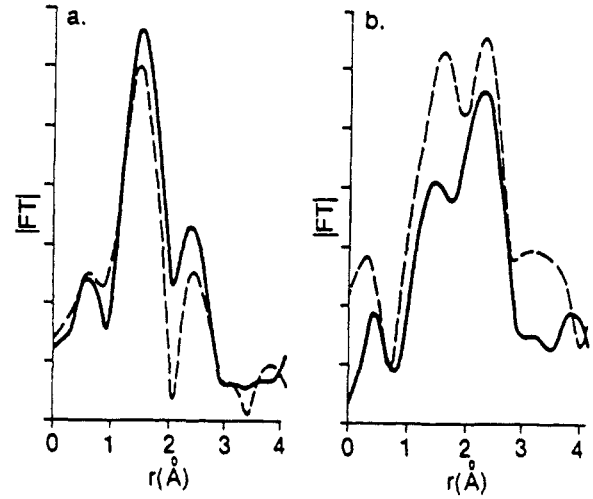


**Figure 20.** Magnitudes of the Fourier transforms for (a) ex situ and (b) in situ passive films on iron substrates. The nitrite-formed film results are given by the dashed lines and the chromate-formed film results by the solid lines. Reprinted from ref 26; copyright 1983 Elsevier.

films passivated in both potassium chromate and sodium nitrite solution using a photocathode X-ray ionization chamber similar to the one shown in Figure 4.[59,60] Although this detection method does not require a vacuum, it does not allow the film to be in contact with solution. Transmission EXAFS was measured on iron foil and $Fe_2O_4$ powder for comparison to the passive films and extraction of the phase functions for bond length determination. The X-ray spectra of the nitrite- and chromate-passivated films appeared quite similar except for the positions of the absorption edges and the near-edge structure. This indicated a difference in the electronic structure of the two films. The phase-corrected Fe–O bond lengths for the nitrite and chromate films were 2.02 and 2.09 ± 0.05 Å, and the Fe–Fe bond lengths were 3.21 and 3.18 ± 0.1 Å, respectively. The Fe–O bond lengths were a bit longer than $Fe_2O_4$, 1.82 Å, and γ-FeOOH, 1.94 Å,[61] and the Fe–Fe bond lengths fell in between $Fe_2O_4$, 3.35 Å, and γ-FeOOH, 2.88 Å. This demonstrates that the structures of the passive films do not strongly resemble the crystalline oxides. It was also observed that the chromate films show a greater degree of disorder as evidenced by the poor Fourier resolution.

In later papers by Long and co-workers[26,62] a similar in situ experiment utilizing the electrochemical cell is described (Figure 11). They demonstrated that a passive film could be formed and maintained under anodic polarization while EXAFS fluorescence measurements were performed. The Fourier transform of the ex situ and in situ experiments for both the nitrite- and chromate-passivated films are shown in Figure 20. The ex situ structures are fairly similar to each other except that the chromate film was less ordered. This was interpreted as due to the incorporation of chromium into the film, resulting in a more "glassy" structure. Significant differences were observed between the in situ and ex situ results and between the in situ nitrite and chromate results. Long and co-workers suggested that the influence of chromium incorporation may be greater in situ and that a protonated species may play an important role in the in situ structure. Hydrogen may be in the form of water, hydroxyl ions,[63] or protons as

determined by radiotracer methods,[64] SIMS,[65] and Mössbauer spectroscopy.[66]

Forty and co-workers have studied passivation of iron–chromium alloys in sodium nitrite using both in situ and ex situ fluorescence EXAFS.[67] They observed that the Fe–O and Fe–Fe bond distances increased as the percent of chromium was increased and that the distances approach those of γ-FeOOH in alloys containing greater than 13 atom % chromium. It is interesting to note that the corrosion resistance of these alloys determined electrochemically improves substantially at or greater than 15 atom % chromium.[68] These authors present evidence for the presence of $Cr_2O_3$ in the high-chromium alloys in addition to the observation that $Cr_2O_3$ seems to stabilize the γ-FeOOH-like structure in the passive film against dehydration.

Hoffman has studied the passivation of iron films in a buffered borate solution at pH 8.4 using the in situ electrochemical cells described in Figures 12 and 13.[27,28] The iron film electrodes were placed in deaerated borate solution and cathodically biased at −350 mV vs a Pd–H reference to remove any air-formed oxide and then stepped to −200 mV to allow hydrogen to escape. Fresh borate solution was added, and the electrode was stepped to +1350 mV vs a Pd–H reference to passivate the iron film. The X-ray spectra were measured by fluorescence. Iron EXAFS indicated that the iron in the passive film had six oxygen neighbors at 2.0 ± 0.1 Å and that there was an absence of bulk crystalline oxides consistent with the other findings. The EXAFS of the passive film was similar to γ-FeOOH gel. There was little contribution from higher shells, which is typical of a disordered structure. The EXAFS of a cathodically protected iron film showed structure typical of bulk iron with no significant oxygen contribution. In situ Mössbauer spectroscopy of these films indicated that the iron in the passive film was in the $Fe^{3+}$ high-spin state and the film had a noncrystalline structure.

## B. Nickel

### 1. Passivation of Nickel

The protective film produced when nickel metal film is passivated in $H_2SO_4$ has been studied in situ by grazing incidence EXAFS.[29,69] The electrochemical cell is shown in Figure 14. The EXAFS of the nickel electrode was compared to that for nickel foil, which was measured by transmittance (Figure 21). Also shown is the nickel electrode after passivation at 417 mV vs SCE in 0.5 M $H_2SO_4$ compared to NiO powder. There is quite good agreement between the nickel electrode and the foil, especially when one considers that the ratio of irradiated volumes is $10^{-3}$:1. In contrast, the passivated nickel electrode exhibits poor oscillations as compared to NiO powder. This indicates that the passive film is rather disordered. Comparison of the near-edge structure before and after passivation demonstrates a change in the oxidation state of the nickel and nearest-neighbor environment.

### 2. Oxidation of $Ni(OH)_2$

In situ transmission EXAFS of nickel hydroxide electrodes has recently been measured.[30] The electrodes were prepared by ball milling nickel hydroxide, cobalt hydroxide, and graphite powder together. The resulting

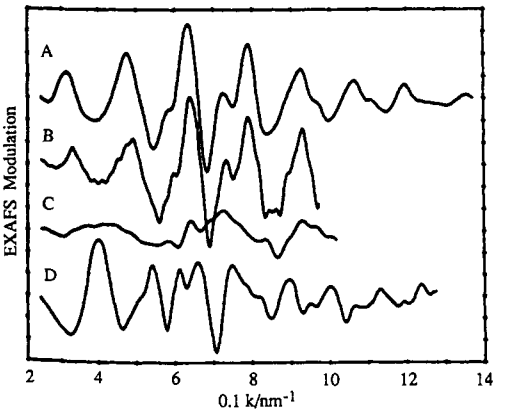


**Figure 21.** EXAFS modulation vs $k$ for a Ni electrode before (B) and after (C) passivation in 0.5 M sulfuric acid, at 0–3.4 mrad. Curves A and D were obtained from transmission measurements on Ni and NiO, respectively, for comparison. Adapted from ref 69.

powder was mixed with chopped vitreous carbon and poly(vinylidene fluoride) in 2-propanol and then cast and pressed onto filter paper. The resulting film was used as the working electrode in the electrochemical cell described in Figure 15. Four electrodes were analyzed: a dry electrode, one oxidized in situ, one oxidized and then reduced back to it original state, and one reoxidized after being oxidized and reduced once. The Fourier transform of all the electrodes showed two main peaks corresponding to Ni–O and Ni–Ni back-scattering. Empirical phase and amplitude functions were derived from nickel foil and NiO standards and used to determine the bond length and coordination number. The bond length and coordination number for the dry electrode were found to agree very well with the X-ray diffraction results from $Ni(OH)_2$.[70] Each nickel is surrounded by six oxygens at a distance of 2.04 Å, and the second shell has six nickel atoms at a distance of 3.16 Å. Oxidation of the $Ni(OH)_2$ electrode causes the Ni–O and Ni–Ni distances to contract to 1.88 and 2.87 Å, respectively. Rereduction and reoxidation of the $Ni(OH)_2$ electrodes result in similar looking EXAFS; however, the disorder of the structure increases with each subsequent redox process, resulting in an increase in the Debye–Waller factor and reduction of the apparent coordination number. It is interesting to note that this disorder facilitates the electrochemical oxidation to the trivalent state.

The EXAFS of NiO electrochemically produced at high temperatures (1273 K) in a solid-state electrochemical cell resulted in a Ni–O distance of 2.08 Å and a Ni–Ni distance of 2.98 Å.[71]

## C. Aluminum Oxidation

The surface EXAFS study of aluminum and its oxides cannot be accomplished in contact with electrolyte due to the low energy of the aluminum edge, which results in high absorption of the X-rays by the electrolyte and air. However, some EXAFS studies of the interaction of oxygen with aluminum under low-pressure conditions have been reported.

The oxidation of aluminum has been determined to proceed in a stepwise fashion. An oxygen exposure of 100 L (langmuir, 1 L = $10^{-6}$ Torr·s) at 2 × $10^{-7}$ Torr results in the chemisorption of molecular oxygen on the surface of aluminum as shown by surface EXAFS and

photoemission. The Al–O bond distance was determined to be 2.22 ± 0.1 Å.[72] When the oxygen exposure was raised to 125 L at 1 × $10^{-6}$ Torr, the molecular oxygen dissociated and coordinated to the 3-fold hollow sites on the aluminum surface. This results in the bond length shortening to 1.92 ± 0.05 Å. In a similar experiment, Johansson[73] and co-workers determined the bond length to be 1.79 ± 0.05 Å. In their experiment two different angles of incidence were used to measure EXAFS, 11° and 45°. The two angles were utilized in order to determine the relative contribution of the oxide phase, 11°, relative to the chemisorbed phase, 45°, at oxygen exposures of 100–150 L at 1 × $10^{-6}$ Torr. The oxide phase is composed of oxygen that has penetrated the surface aluminum layer and, as concluded in this work, preferentially goes into tetrahedral interlattice positions. The bond length of 1.79 Å is consistent with the oxygen residing in the tetrahedral holes of aluminum. If the oxygen atoms were in the octahedral holes, the bond length would be 2.02 Å. This is in contrast to the calculations by Bylander and Kleinman[74] in which they found that the maximum binding energy for this system occurs when one oxygen is placed at the center of a distorted octahedron and another in a 3-fold site on the surface directly above it. At higher oxygen exposures, 1000 L, and temperature, an increase in the bond length from 1.79 to 1.88 ± 0.05 Å was observed by Johansson and co-workers. They interpreted this as a result of the oxygen atoms penetrating the aluminum surface and bonding with second- and third-layer aluminum atoms, resulting in a disordered amorphous phase.

Photoemission extended X-ray absorption fine structure was used by Kim et al. to study aluminum oxidation at 25- and 1000-L exposures.[75] They concluded that oxygen is located in 3-fold sites in or close to the Al(111) planes at a distance of 1.76 Å.

## D. Copper Oxidation

Copper forms two oxides when it is heated in air. At 200 °C a layer of $Cu_2O$ is formed as indicated by the characteristic red color. At 300 °C black CuO is formed. This has been demonstrated by Fischer et al.[13] using surface EXAFS obtained by measuring the Auger electrons emitted upon absorption of X-rays (see Figure 4). Samples were prepared by heating freshly sanded copper plates for 1 h in air at 200 and 300 °C to obtain the red $Cu_2O$ and black CuO. Spectra of pure $Cu_2O$ and CuO powders were measured by transmittance for comparison. Figure 22 demonstrates the similarity between copper plate heated at 200 °C and $Cu_2O$ and copper plate heated at 300 °C and CuO powder. This supports the idea that $Cu_2O$ forms first as an intermediate during the oxidation of copper. The fact that the oxidized copper plates show the pure oxides suggests that a homogeneous oxide layer of at least 1000 Å forms parallel to the surface. This is based on the fact that the X-rays can only penetrate beneath the surface at most 1000 Å at the angle of incidence of 1°. Oxidation of copper in parallel layers has previously been observed by Czanderna[76] using TEM.

## E. Adsorbed Iodine on Platinum

Iodine forms an ordered chemisorbed monolayer on the surface of the platinum which is relatively insensitive to contamination.[77] The structure of this layer and the effect electrolyte has on it were determined by surface EXAFS.[78] A single crystal of Pt(111) was polished and cleaned by oxygen sputtering followed by annealing under vacuum. The platinum crystal was then exposed to iodine vapor. Surface EXAFS was measured at grazing incidence with an energy-dispersive high-purity germanium detector using soller slits and antimony filters.

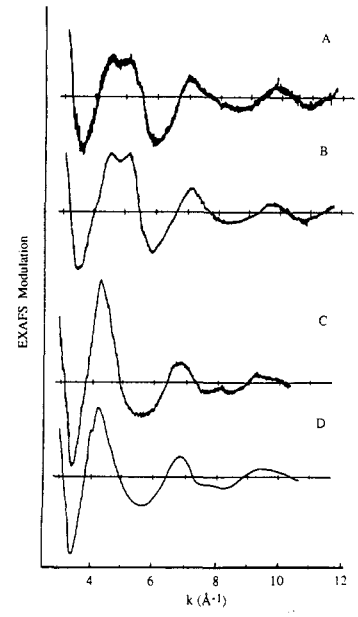


**Figure 22.** EXAFS modulation vs $k$ measured (A) from the surface of a freshly sanded Cu plate heated to 200 °C in air for 1 h, (B) of $Cu_2O$ powder, (C) from the surface of a freshly sanded Cu plate that had been heated to 300 °C in air for 1 h, and (D) of CuO powder. Adaopted from ref 13.

In a nitrogen atmosphere, a well-defined iodine absorption edge was observed at 33.16 keV. Several scans were averaged to obtain a suitable signal to noise ratio. The main peak in the Fourier transform corresponds to a Pt–I distance of 2.63 Å after phase correction. This peak can be assigned to Pt–I and not I–I back-scattering because the I–I bond axis is perpendicular to the E vector of the X-ray beam. As a result, I–I back-scattering does not contribute to the EXAFS signal.

The crystal was then immersed in 0.1 M $NaClO_4$ solution and partially withdrawn. The X-ray beam was focused onto the solution meniscus. A loss in signal of 10–15% was observed as compared to the ex situ experiment. Analysis of the spectra yielded similar results, giving a bond length of 2.64 Å for the Pt–I bond distance. This experiment demonstrated the potential of EXAFS to measure a monoatomic layer at the metal–liquid interface.

The ex situ surface EXAFS studies of iodine on Ag(111)[79] and on both Cu(111) and Cu(100)[80] have also been reported.

## F. Underpotentially Deposited (UPD) Films

### 1. Introduction

A monolayer of a metal film can be deposited at a potential that can be several hundred millivolts less negative than its thermodynamic deposition potential. Once the monolayer is formed, no more deposition occurs unless the electrode is biased negative of the

thermodynamic deposition potential. In the following discussions, the electrodes were "potentially clamped" at a potential between that of the formation of the UPD monolayer and bulk deposition in order to maintain a stable surface coverage during the course of the EXAFS experiment. In all cases the surface EXAFS was measured at grazing incidence (see section II). As a result of the E vector of the X-ray beam being polarized perpendicular to the surface of the electrode, interatomic vectors in the plane of the electrode do not contribute to the EXAFS signal. The electrochemical cell used in these experiments is shown in Figure 10.

### 2. Copper Films

**a. On Gold.** A monolayer of copper was underpotentially deposited in situ at 130 mV vs Ag/AgCl on a gold electrode from a $2 \times 10^{-5}$ M $CuSO_4$ solution containing 1 M $H_2SO_4$ as a supporting electrolyte.[81] The gold electrode was prepared by epitaxially depositing Au(111) onto a cleaved mica substrate. The X-ray spectrum of UPD copper was compared to spectra of aqueous $CuSO_4$ and CuAu alloy. The absorption edge of $Cu^{2+}$(aq) was 4 eV higher in energy than the UPD copper film, and it had a very sharp near-edge peak with strongly damped EXAFS. The damped EXAFS indicates a large Debye–Waller factor as a result of the loosely bound hydration shell. The CuAu alloy X-ray spectrum was also much different from that of the UPD copper film. The CuAu alloy had a small double peak in the near-edge region and a number of well-defined oscillations in the EXAFS region of the spectrum.

The best fit of the UPD copper film data was obtained when both Au and O back-scatterers were used. It was proposed that the signal arises from copper bonded to three gold atoms at the metallic surface, forming an elongated tetrahedron or octahedron with oxygen coordination from either water or sulfate ion on the top of the copper atom. The resulting bond length for Cu–Au was 2.5 Å and for Cu–O, 2.05 or 2.08 Å depending whether the oxygen was modeled by one atom from water or three oxygens atoms from sulfate ion coordination, respectively. No Cu–Cu interaction was observed as a result of the polarization of the X-ray beam perpendicular to the plane of the electrode surface.

In a more recent paper,[82] the EXAFS results were described for the X-ray polarization parallel to the surface of the electrode. Back-scattering was only observed for the Cu–Cu and Cu–Au neighbors. The Cu–Cu and Cu–Au distances were determined to be 2.92 ± 0.03 and 2.58 ± 0.03 Å, respectively. The Cu–Cu distance is consistent with the Au–Au spacing in the (111) plane, 2.89 Å. This suggests that the copper forms a commensurate adlayer on the gold surface. The Cu–Au distance was in good agreement with the results from the perpendicular X-ray polarization experiment. The absence of Cu–O back-scattering indicates that the oxygen occupies sites directly on top of the copper atoms in the adlayer. If the oxygen took up a bridge position, it would have a contribution to the EXAFS signal when the beam polarization is parallel to the electrode surface.

**b. On Platinum.** Copper has also been underpotentially deposited from a 0.05 mM $Cu^{2+}$ solution in 0.1 M sulfuric acid onto a iodine-treated Pt(111) electrode and studied in situ by EXAFS.[83] In this experiment, the X-ray polarization was parallel to the electrode surface. The Fourier transform of the EXAFS data yielded one large peak at 2.45 Å corresponding to Cu–Cu back-scattering. The Cu–Cu distance after phase shift correction was determined to be 2.88 ± 0.04 Å, and the coordination number was found to be similar to that of copper foil if copper was assumed to be the only neighbor. Other studies of this system have demonstrated that the copper atoms displace the iodine on the surface of the platinum electrode and that the iodine resides on the copper metal layer.[84] As a result of the polarization of the X-ray beam, iodine back-scattering contributes little to the X-ray spectrum. The copper adlattice was expanded as compared to the platinum substrate (2.88 vs 2.75 Å). This results in a range of Cu–Pt distances that causes the EXAFS signal from Cu–Pt back-scattering to be damped. The packing density of the copper in the platinum surface was found to be 0.33 as determined by electrochemical stripping. With a coverage of 0.33 the mean coordination number would be approximately 2 if the copper atoms were evenly distributed over the electrode surface; thus, the copper, which displays a much higher number of back-scatterers, must be forming clusters on the platinum surface.

### 3. Silver on Gold

A 2500-Å Au(111) film was epitaxially grown onto a cleaved ruby mica surface and used as the working electrode.[85] A monolayer of silver was underpotentially deposited in situ at 600 mV vs. Ag/AgCl onto the gold electrode from a solution of $5 \times 10^{-5}$ M $Ag^+$ and 0.1 M $HClO_4$ supporting electrolyte. During the EXAFS experiment a ~30-$\mu$m-thick layer of electrolyte was present. Well-defined voltammograms were obtained in this thin-layer configuration at a scan rate of 1 mV/s.

The raw X-ray spectrum displayed a well-defined Ag K edge rise at 25.5 keV; however, significant edge features were not readily visible and the EXAFS was weak. Weak EXAFS can be attributed to inelastic scattering, thermal vibrations, and static disorder.[5a]

The EXAFS data were shown to be consistent with having both gold and oxygen back-scatterers in a ratio of 3:1, respectively. From this, it was proposed that a silver atom sits in a 3-fold site on the gold surface and is bonded to an oxygen from either water or perchlorate, much like that observed for the copper on gold system. The bond lengths were found to be 2.75 and 2.42 ± 0.05 Å for Ag–Au and Ag–O, respectively. However, the Ag–Au bond length is somewhat shorter than that which is consistent with the Ag–Au alloy length of 2.88 Å.[86] The Ag–O distance is also marginally longer than the expected value of 2.30 Å. The reason for this was not understood.

### 4. Lead on Silver

A monolayer of lead was underpotentially deposited at −530 mV vs Ag/AgCl onto a Ag(111) electrode.[25] The silver electrode was prepared by epitaxially depositing 2500 Å of silver onto a cleaved mica surface. The electrolyte contained 0.5 M sodium acetate, 0.1 M acetic acid, and $5 \times 10^{-5}$ M lead acetate. The structure of the UPD lead films was studied at −530 and −1000 mV vs Ag/AgCl.

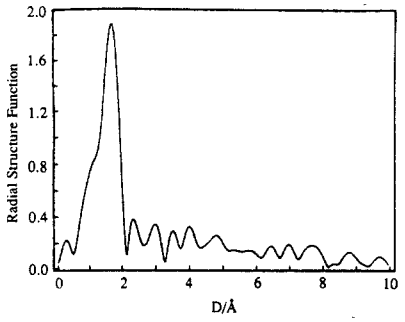


**Figure 23.** Radial structure function of UPD Pb on Ag(111) under potential control at −0.53 V vs Ag/AgCl. Reprinted from ref 25; copyright 1987 American Chemical Society.

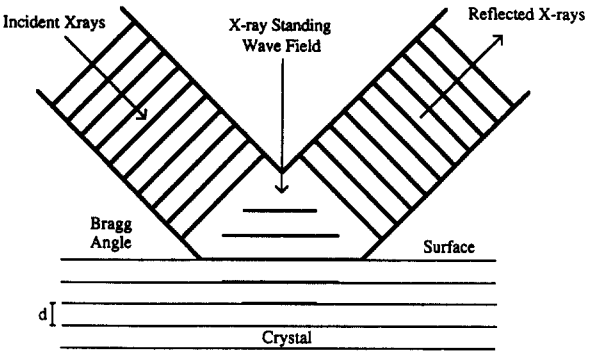


**Figure 24.** Generation of an X-ray standing wave field. Adapted from ref 51.

The near-edge spectra of the UPD lead film were compared to aqueous lead acetate, $PbO_2$, and lead foil. The absorption edge of the UPD lead monolayer was found to be the same as for lead foil. The absorption edges of lead acetate and $PbO_2$ were found to be shifted 1.2 and 2.2 eV to higher energy, respectively, as compared to the UPD lead film, suggesting that the lead in the electrochemical cell is completely reduced. The near-edge spectrum of the UPD film has a small shoulder at the onset of the absorption edge that is not present in the lead foil or lead acetate spectrum. However, the spectrum for $PbO_2$ displays a similar but larger shoulder. This shoulder is very likely associated with oxygen coordination to the UPD lead film.

The Fourier transform of the EXAFS of the UPD lead film at −530 mV is shown in Figure 23. Only one major peak is observed at 1.76 Å, which is believed to correspond to Pb–O back-scattering. The FT of the EXAFS for a Pb–Ag alloy displays a peak at 2.64 Å corresponding to Pb–Ag back-scattering. Two possible explanations were given for the lack of a Pb–Ag peak for the UPD lead film. First, lead has a low melting point (600 K), which would result in a large Debye–Waller factor. The polycrystalline lead foil used for edge comparisons also did not yield any EXAFS. In addition, the melting point of a lead monolayer on a copper single crystal was reported to be lower than the bulk lead melting point.[87] It is expected that a similar melting point depression would occur on silver. Second, the UPD lead film is expected to form an incommensurate structure on top of a Ag(111) surface as a result of the difference in atomic radii between lead and silver (1.74 and 1.44 Å, respectively). This could result in multiple Pb–Ag distances giving rise to oscillations of a variety of frequencies causing a damping of the EXAFS signal from Pb–Ag back-scattering.

The Pb–O bond distance at −530 mV was determined to be 2.33 ± 0.02 Å as compared to the shorter distance in $PbO_2$ of 2.16–2.22 Å. The Debye–Waller factor is much smaller than expected for the Pb–O back-scattering, indicating that the adsorbed oxygen atoms occupy specific sites at the lead surface. The Pb–O bond distance was observed to increase by 0.05 Å (2.38 ± 0.02 Å) when the electrode potential was stepped to −1000 mV.

Further investigation of this system is discussed in a subsequent paper in which grazing incidence X-ray scattering measurements were used to follow the in situ growth of a lead film.[88] In this work, a monolayer of Pb was found to form a close-packed triangular lattice on the silver electrode that was compressed 1.4% relative to bulk lead. This strain was observed to increase with a more cathodic deposition potential. As a result of the strain, lead cannot be epitaxially grown on silver, which is consistent with the lack of Ag–Pb back-scattering in the EXAFS experiment.

## VII. Use of X-ray Standing Waves for Electrode Interfacial Studies

X-ray standing waves have been shown to be a very sensitive tool for the study of electrode interfaces.[51,89-91] The X-ray standing waves result from interference between the coherently related incident and Bragg-diffracted beam from a high-quality crystal. This standing wave extends beyond the crystal surface, allowing one to study a material on the surface of the crystal. The length of the wave is determined by the d spacing of the diffracting planes in the crystal. Figure 24 demonstrates how an X-ray standing wave is formed. Standing waves can be used to probe the amount of material on the surface of a crystal, the relative distance between the crystal surface and material immobilized on the crystal, and the degree of order in the material on the crystal surface. The crystal is rocked about the Bragg reflection angle, which causes the nodal and antinodal planes of the standing wave to move through the atom plane of the surface material. This causes the fluorescence emission yield from the surface material to be modulated. The phase and amplitude of this modulation are a result of the mean position and width of the heavy atoms on the crystal surface. Nearly perfect crystals of metals are difficult to obtain so these experiments have been performed using layered synthetic microstructures (LSMs), which are prepared by the deposition of alternate layers of materials onto a smooth substrate.

The electrochemical deposition of copper in an iodide-coated platinum/carbon LSM has been investigated by X-ray standing waves.[89] The resulting data indicated that the copper layer was closer to the platinum surface than the iodide layer, suggesting that the iodide layer was displaced by copper during deposition. The potential dependence of the adsorption of iodide on a Pt/C LSM has also been studied with use of X-ray standing waves.[51] The technique has also been applied to polymer systems. The electropolymerized polymer $[Ru(v\text{-}bpy)_3]^{2+}$ (see section V.C) was found to be deposited onto a W/C LSM in ordered layers.[90] Materlik et al. have used standing waves to study Tl underpotentially deposited (UPD) on high-quality Cu(111) single crystals.[91] The deposition was performed in

aqueous 0.5 M $Na_2SO_4$ and $10^{-3}$ M $TlNO_3$ between −0.7 and −0.6 V vs SCE in both oxygen-free and oxygen-contaminated electrolyte. Standing wave studies of the Tl UPD films grown in the oxygen-free electrolyte were consistent with the Tl atoms occupying a 2-fold position on the Cu(111) surface with a contraction of the metallic Tl radius by 3%. Standing wave studies of the Tl UPD films grown in the oxygen-contaminated electrolyte indicated reconstruction of the Cu surface atoms by adsorption of oxygen, causing an inward shift of the copper surface atoms by about 0.3 Å. The Tl atoms are then absorbed onto the oxygen-reconstructed surface. These structures were found to be stable after exposure to the atmosphere, suggesting that the Tl layer prevents direct oxidation of the Cu surface.

X-ray standing waves are well suited for the study thin films of heavy-atom-containing materials immobilized on electrode surfaces. Unfortunately, the experiments are very difficult and require materials not yet widely available.

## VIII. Conclusion

The EXAFS spectroelectrochemical technique has been successfully utilized for a variety of applications from bulk-solution to thin-film studies. The use of an electrochemical technique to convert and maintain a species in a particular oxidation state in conjunction with X-ray absorption spectroscopy allows the study of changes in the coordination environment around an absorbing center as a function of oxidation state. Protecting a species in a given oxidation state during the X-ray absorption spectroscopy experiment is very important since hydrated electrons are produced by the interaction of water with the X-rays. Without the constant-potential bias, some of the species of interest could be reduced during the X-ray measurements, yielding uninterpretable results. The other major advantage of this technique is its ability to be used for in situ structural studies, thus avoiding the problem of possible decomposition and structural rearrangement upon removal of the sample from solution.

## References


(1) Heineman, W. R.; Hawkridge, F. M.; Blount, H. N. In *Electroanalytical Chemistry*; Bard, A. J., Ed.; Dekker: New York, 1984; Vol. 13, pp 1–113.
(2) Gale, R. J., Ed. *Spectroelectrochemistry: Theory and Practice*; Plenum: New York, 1988.
(3) McCreery, R. L. In *Physical Methods of Chemistry*; Rossiter, B. W., Hamilton, J. F., Eds.; Wiley: New York, 1986; Vol. 2, Chapter 7.
(4) Hoffman, R. W. In *Passivity of Metals and Semiconductors*; Froment, M., Ed.; Elsevier: Amsterdam, 1983; p 147.
(5) (a) Teo, B. K. *EXAFS: Basic Principles and Data Analysis*; Springer-Verlag: Berlin, 1986. (b) Cramer, S. P.; Hodgson, K. O. *Prog. Inorg. Chem.* **1979**, *25*, 1. (c) Eisenberger, P.; Kincaid, B. M. *Science* **1978**, *200*, 1441. (d) Fay, M. J.; Procter, P.; Hoffmann, D. P.; Hercules, D. M. *Anal. Chem.* **1989**, *60*, 1225A.
(6) (a) Sham, T. K.; Hastings, J. B.; Perlman, M. L. *J. Am. Chem. Soc.* **1980**, *102*, 5904. (b) Sham, T. K.; Brunschwig, B. S. *J. Am. Chem. Soc.* **1980**, *103*, 1590. (c) Brunschwig, B. S.; Creutz, C.; Macartney, D. H.; Sham, T. K.; Sutin, N. *Faraday Discuss. Chem. Soc.* **1982**, *74*, 113. (d) Sham, T. K. *Acc. Chem. Res.* **1986**, *19*, 99. (e) Sham, T. K. *Topics in Current Chemistry*; Springer-Verlag: Berlin, Heidelberg, 1988; Vol. 145, p 81.
(7) Veigele, W. M. J. *At. Data* **1973**, *5*(1), 64.
(8) Smith, D. A.; Elder, R. C.; Heineman, W. R. *Anal. Chem.* **1985**, *57*, 2361.
(9) Lytle, F.; Greegor, R. B.; Sandstrom, D. R.; Marques, E. C.; Wong, J.; Spiro, C. L.; Huffman, G. D.; Huggins, F. E. *Nucl. Instrum. Methods Phys. Res.* **1984**, *226*, 542.
(10) Stern, E. A.; Heald, S. M. *Rev. Sci. Instrum.* **1979**, *50*, 1579.
(11) Heald, S. M.; Keller, E.; Stern, E. A. *Phys. Lett.* **1984**, *103A*, 155.
(12) Shevchik, N. J.; Fischer, D. A. *Rev. Sci. Instrum.* **1979**, *50*, 577.
(13) Fischer, D. A.; Cohen, G. G.; Shevchik, N. J. *J. Phys. F: Met. Phys.* **1980**, *10*, L139.
(14) Tourillon, G.; Dartyge, E.; Dexpert, H.; Fontaine, A.; Jucha, A.; Lagarde, P.; Sayers, D. E. *J. Electroanal. Chem. Interfacial Electrochem.* **1984**, *178*, 357.
(15) Dartyge, E.; Fontaine, A.; Tourillon, G.; Cortes, R.; Jucha, A. *Phys. Lett.* **1986**, *113A*, 384.
(16) Bosio, L.; Cortes, R.; Defrain, A.; Froment, M.; Lebrun, A. M. In *Passivity of Metals and Semiconductors*; Froment, M., Ed.; Elsevier: Amsterdam, 1983; p 131.
(17) Dewald, H. D.; Watkins, J. W., II; Elder, R. C.; Heineman, W. R. *Anal. Chem.* **1986**, *58*, 2968.
(18) DeAngelis, T. P.; Heineman, W. R. *J. Chem. Educ.* **1976**, *53*, 594.
(19) (a) Heineman, W. R.; Norris, B. J.; Goelz, J. F. *Anal. Chem.* **1975**, *47*, 79. (b) Murray, R. W.; Heineman, W. R.; O'Dom, G. W. *Anal. Chem.* **1967**, *39*, 1666.
(20) Sharpe, L. R.; Kirchhoff, J. R.; Lunte, C. E.; Dewald, H. D.; Elder, R. C.; Heineman, W. R. Manuscript in preparation.
(21) Elder, R. C.; Lunte, C. E.; Rahman, A. F. M. M.; Kirchhoff, J. R.; Dewald, H. D.; Heineman, W. R. *J. Electroanal. Chem. Interfacial Electrochem.* **1988**, *240*, 361.
(22) Albarelli, M. J.; White, J. H.; Bommarito, G. M.; McMillan, M.; Abruna, H. D. *J. Electroanal. Chem. Interfacial Electrochem.* **1988**, *248*, 77.
(23) Albarelli, M. J.; White, J. H.; McMillan, M.; Bommarito, G. M.; Abruna, H. D. In *Electrochemical Surface Science*; Soriaga, M. P., Ed.; ACS Symposium Series 378; American Chemical Society: Washington, DC, 1988; p 216.
(24) Tourillon, G.; Artyge, E.; Fontaine, A.; Jucha, A. *Phys. Rev. Lett.* **1986**, *57*, 603.
(25) Samant, M. G.; Borges, G. L.; Gordon, J. G., II; Melroy, O. R.; Blum, L. *J. Am. Chem. Soc.* **1987**, *109*, 5970.
(26) Long, G. G.; Kruger, J.; Kuriyama, M. In *Passivity of Metals and Semiconductors*; Froment, M., Ed.; Elsevier: Amsterdam, 1983; p 139.
(27) Hoffman, R. W. In *Passivity of Metals and Semiconductors*; Froment, M., Ed.; Elsevier: Amsterdam, 1983; p 147.
(28) Kordesch, M. E.; Hoffman, R. W. *Nucl. Instrum. Methods Phys. Res.* **1984**, *222*, 347.
(29) Bosio, L.; Cortes, R.; Froment, M. In *EXAFS and Near Edge Structure III*; Hodgson, K. O., Hedman, B., Penner-Hahn, J. E., Eds.; Springer-Verlag: Berlin, 1984; p 484.
(30) McBreen, J.; O'Grady, W. E.; Pandya, K. I.; Hoffman, R. W.; Sayers, D. E. *Langmuir* **1987**, *3*, 428.
(31) Heineman, W. R. *J. Chem. Educ.* **1983**, *60*, 305.
(32) Heineman, W. R.; Anderson, W. C.; Halsall, H. B.; Hurst, M. M.; Johnson, J. M.; Kreishman, G. P.; Norris, B. J.; Simone, M. J.; Su, C.-H. In *Electrochemical and Spectrochemical Studies of Biological Redox Components*; Kadish, K. M., Ed.; Advances in Chemistry Series 201; American Chemical Society: Washington, DC, 1982; pp 1–21.
(33) (a) Sutin, N. *Prog. Inorg. Chem.* **1983**, *30*, 441. (b) Endicott, J. *Prog. Inorg. Chem.* **1983**, *30*, 141. (c) Creutz, C. *Prog. Inorg. Chem.* **1983**, *30*, 1.
(34) Smith, D. A.; Heeg, A. J.; Heineman, W. R.; Elder, R. C. *J. Am. Chem. Soc.* **1984**, *106*, 3053.
(35) Teo, B. K. *J. Am. Chem. Soc.* **1981**, *103*, 3990.
(36) Figgis, B. N.; Skelton, B. W.; White, A. H. *Aust. J. Chem.* **1978**, *31*, 1195.
(37) Chance, B.; Angiolillo, P.; Yang, E. K.; Powers, L. *FEBS Lett.* **1980**, *112*, 178.
(38) Korszun, Z. R.; Moffat, K.; Frank, K.; Cusanovich, M. A. *Biochemistry* **1982**, *21*, 2253.
(39) Tourillon, G. In *Handbook of Conducting Polymers*; Skotheim, T., Ed.; Marcel Dekker: New York, 1986; p 294.
(40) Tourillon, G.; Fontaine, A. *Phys. Rev. B: Condens. Matter* **1987**, *35*, 9863.
(41) Tourillon, G.; Dartyge, E.; Fontaine, A.; Garrett, R.; Sagurton, M.; Xu, P.; Williams, G. P. *Europhys. Lett.* **1987**, *4*, 1391.
(42) Tourillon, G.; Flank, A. M.; Lagarde, P. *J. Phys. Chem.* **1988**, *92*, 4397.
(43) Tourillon G.; Fontaine, A.; Jugnet, J.; Tran Minh Duc; Braun, W.; Feldhaus, J.; Holub-Krappe, E. *Phys. Rev. B* **1987**, *36*, 3483.
(44) Tourillon, G.; Dexpert, H.; Lagarde, P. *J. Electrochem. Soc.* **1987**, *134*, 327.
(45) Tourillon, G.; Dartyge, E.; Fontaine, A.; Jucha, A.; Andrieux, C. *J. Phys., Colloq.* **1986**, *2*, C8-551.
(46) Dartyge, E.; Fontaine, A.; Tourillon, G.; Jucha, A. *J. Phys., Colloq.* **1986**, *2*, C8-607.

(47) Tourillon, G.; Dartyge, E.; Dexpert, H.; Fontaine, A.; Jucha, A.; Lagarde, P.; Sayers, D. E. *Surf. Sci.* **1985**, *156*, 536.
(48) Tourillon, G.; Garnier, F. *J. Phys. Chem.* **1983**, *87*, 2289.
(49) Murray, R. W. *Acc. Chem. Res.* **1980**, *13*, 135.
(50) Szentrimay, M. N.; Martin, C. R. *Anal. Chem.* **1984**, *56*, 1898.
(51) Abruna, H. D.; White, J. H.; Albarelli, M. J.; Bommarito, M. G.; Bedzyk, M. J.; McMillan, M. *J.Phys. Chem.* **1988**, *92*, 7045.
(52) (a) Abruna, H. D.; Denisevich, P.; Umana, M.; Meyer, T. J.; Murray, R. W. *J. Am. Chem. Soc.* **1981**, *103*, 1. (b) Denisevich, P.; Abruna, H. D.; Leidner, C. R.; Meyer, T. J.; Murray, R. W. *Inorg. Chem.* **1982**, *21*, 2153. (c) Ghosh, P. K.; Spiro, T. G. *J. Electrochem. Soc.* **1981**, *128*, 1281.
(53) Rillema, D. P.; Jones, D. S.; Levy, H. A. *J. Chem. Soc., Chem. Commun.* **1979**, 849.
(54) Van'T Blik, H. F. J.; Koningsberger, D. C.; Prins, R. *J. Catal.* **1986**, *97*, 210.
(55) Resasco, D. E.; Weber, R. S.; Sakellson, S.; McMillan, M.; Haller, G. L. *J. Phys. Chem.* **1988**, *92*, 189.
(56) Koningsberger, D. C.; Duivenvoorden, F. B. M.; Kip, B. J.; Sayers, D. E. *J. Phys., Colloq.* **1986**, *47*, C8-255.
(57) Moller, K.; Bein, T. *J. Phys., Colloq.* **1986**, *47*, C8-231.
(58) Exner, D.; Jaeger, N. I.; Moller, K.; Schulz-Ekloff, G. *J. Chem. Soc., Faraday Trans. 1* **1982**, *78*, 3537.
(59) Long, G. G.; Kruger, J.; Black, D. R.; Kuriyama, M. *J. Electroanal. Chem. Interfacial Electrochem.* **1983**, *150*, 603.
(60) Long, G. G.; Kruger, J.; Black, D. R.; Kuriyama, M. *J. Electrochem. Soc.* **1983**, *130*, 240.
(61) Wyckoff, R. W. G. *Crystal Structures*, 2nd ed.; Wiley: New York, 1963; Vol. 1.
(62) Kruger, J.; Long, G. G.; Kuriyama, M.; Goldman, A. I. In *Passivity of Metals and Semiconductors*; Froment, M., Ed.; Elsevier: Amsterdam, 1983; p 163.
(63) Noda, T.; Kudo, K.; Sato, N. *Z. Phys. Chem.* **1975**, *98*, 271.
(64) Yolken, H. T.; Kruger, J.; Calvert, J. P. *Corros. Sci.* **1968**, *8*, 103.
(65) Murphy, D. J.; Bockris, J. O'M.; Pou, T. E.; Cocke, D. L.; Sparrow, G. *J. Electrochem. Soc.* **1982**, *129*, 2149.
(66) O'Grady, W. F. *J. Electrochem. Soc.* **1980**, *127*, 555.
(67) Forty, A. J.; Kerkar, M.; Robenson, J.; Ward, M. *J. Phys., Colloq.* **1986**, *47*, C8-1077.
(68) Revesz, A. G.; Kruger, J. In *Passivity of metals*; Frankenthal, R. P., Kruger, J., Eds.; The Electrochemical Society: Princeton, 1978; p 137.
(69) Bosio, L.; Cortes, R.; Defrain, A.; Froment, M. *J. Electroanal. Chem. Interfacial Electrochem.* **1984**, *180*, 265.
(70) McEwen, R. S. *J. Phys. Chem.* **1971**, *75*, 1782.
(71) Tomellini, M.; Gozzi, D.; Bianconi, A.; Davoli, I. *J. Chem. Soc., Faraday Trans. 1* **1987**, *83*, 289.
(72) Bachrach, R. Z.; Hansson, G. V.; Bauer, R. S. *Surf. Sci.* **1981**, *109*, L560.
(73) Johansson, L. I.; Stohr, J.; Brennan, S. *App. Surf. Sci.* **1980**, *6*, 419.
(74) Bylander, D. M.; Kleinman, L. *Phys. Rev. B* **1984**, *30*, 2997.
(75) Kim, S. T.; Choudhary, K. M.; Shah, S. N.; Lee, J. H.; Rothberg, G. M.; denBoer, M. L.; Williams, G. P. *J. Vac. Sci. Technol. A* **1987**, *5*, 623.
(76) Czanderna, A. W. *J. Vac. Sci. Technol.* **1972**, *9*, 393.
(77) Felter, T. E.; Hubbard, A. T. *J. Electroanal. Chem. Interfacial Electrochem.* **1979**, *100*, 473.
(78) Gordon, J. G., II; Melroy, O. R.; Borges, G. L.; Reisner, D. L.; Abruna, H. D.; Chandrasekhar, P.; Blum, L. *J. Electroanal. Chem. Interfacial Electrochem.* **1986**, *210*, 311.
(79) Citrin, P. H.; Eisenberger, P.; Hewitt, R. C. *Phys. Rev. Lett.* **1978**, *41*, 309.
(80) Citrin, P. H.; Eisenberger, P.; Hewitt, R. C. *Phys. Rev. Lett.* **1980**, *45*, 1948.
(81) Blum, L.; Abruna, H. D.; White, J.; Gordon, J. G., II; Borges, G. L.; Samant, M. G.; Melroy, O. R. *J. Chem. Phys.* **1986**, *85*, 6732.
(82) Melroy, O. R.; Samant, M. G.; Borges, G. L.; Gordon, J. G., II; White, J. H.; Albarelli, M. J.; McMillan, M.; Abruna, H. D. *Langmuir* **1988**, *4*, 728.
(83) White, J. H.; Abruna, H. D. *J. Electroanal. Chem. Interfacial Electrochem.* In press.
(84) (a) Stickney, J. L.; Rosasco, S. D.; Hubbard, A. T. *J. Electrochem. Soc.* **1984**, *131*, 260. (b) Bedzyk, M. J.; Bilderback, D. H.; White, J. H.; Bommarito, G. M.; Abruna, H. D. *J. Phys. Chem.* **1986**, *90*, 4926.
(85) White, J. H.; Albarelli, M. J.; Abruna, H. D.; Blum, L.; Melroy, O. R.; Samant, M. G.; Borges, G. L.; Gordon, J. G. II. *J. Phys. Chem.* **1988**, *92*, 4432.
(86) Pearson, W. P. *Handbook of Lattice Spacings and Structures of Metals and Alloys*; Pergamon: New York, 1958.
(87) Henrion, J.; Rhead, G. E. *Surf. Sci.* **1972**, *29*, 20.
(88) Melroy, O. R.; Toney, G. L.; Borges, G. L.; Samant, M. G.; Kortright, J. B.; Ross, P. N.; Blum, L. *J. Electroanal. Chem. Interfacial Electrochem.* **1989**, *258*, 403.
(89) Bedzyk, M. J.; Bilderback, D.; White, J.; Abruna, H. D.; Bommarito, M. G. *J. Phys. Chem.* **1986**, *90*, 4926.
(90) White, J. H.; Albarelli, M. J.; Bommarito, M. G.; Abruna, H. D. Report TR-6; Order No. AD-A183521, 13 pp. Available NTIS from: *Gov. Rep. Announce. Index (U.S.)* **1987**, *87* (23), Abstr. No. 753,455.
(91) Materlik, G.; Zegenhagen, J.; Uelhoff, W. *Phys. Rev. B* **1985**, *32*, 5502.